Available online at www.sciencedirect.com
SCIENCE DIRECT®
ELSEVIER
Tectonophysics 410 (2005) 389–415
TECTONOPHYSICS
www.elsevier.com/locate/tecto

On the mechanics of basin formation in the Pannonian basin: Inferences from analogue and numerical modelling

Gábor Windhoffer [a,✠], Gábor Bada [a,b,*], Dick Nieuwland [b,c], Géza Wórum [b,d], Ferenc Horváth [a], Sierd Cloetingh [b]

[a] *Institute of Geography and Earth Sciences, Eötvös Loránd University, Pázmány P. s. 1/C, 1117 Budapest, Hungary*
[b] *Netherlands Research Centre for Integrated Solid Earth Science (ISES), Vrije Universiteit Amsterdam, De Boelelaan 1085, 1081 HV Amsterdam, the Netherlands*
[c] *NewTec Ltd., 4e Binnenvestgracht 13, 2311 NT Leiden, the Netherlands*
[d] *Geomega Ltd., Mester u. 4, 1095 Budapest, Hungary*

Received 16 March 2004; accepted 19 October 2004
Available online 25 October 2005

Abstract

We present the results of a thrust fault reactivation study that has been carried out using analogue (sandbox) and numerical modelling techniques. The basement of the Pannonian basin is built up of Cretaceous nappe piles. Reactivation of these compressional structures and connected weakness zones is one of the prime agents governing Miocene formation and Quaternary deformation of the basin system. However, reactivation on thrust fault planes (average dip of ca. 30°) in normal or transtensional stress regimes is a problematic process in terms of rock mechanics. The aim of the investigation was to analyse how the different stress regimes (extension or strike-slip), and the geometrical as well as the mechanical parameters (dip and strike of the faults, frictional coefficients) effect the reactivation potential of pre-existing faults.

Results of analogue modelling predict that thrust fault reactivation under pure extension is possible for fault dip angle larger than 45° with normal friction value (sand on sand) of the fault plane. By making the fault plane weaker, reactivation is possible down to 35° dip angle. These values are confirmed by the results of numerical modelling. Reactivation in transtensional manner can occur in a broad range of fault dip angle (from 35° to 20°) and strike angle (from 30° to 5° with respect to the direction of compression) when keeping the maximum horizontal stress magnitude approximately three times bigger than the vertical or the minimum horizontal stress values.

Our research focussed on two selected study areas in the Pannonian basin system: the Danube basin and the Derecske trough in its western and eastern part, respectively. Their Miocene tectonic evolution and their fault reactivation pattern show considerable differences. The dominance of pure extension in the Danube basin vs. strike-slip faulting (transtension) in the Derecske trough is interpreted as a consequence of their different geodynamic position in the evolving Pannonian basin system. In addition, orientation of the pre-existing thrust fault systems with respect to the Early to Middle Miocene paleostress fields had a major influence on reactivation kinematics.

As part of the collapsing east Alpine orogen, the area of the Danube basin was characterised by elevated topography and increased crustal thickness during the onset of rifting in the Pannonian basin. Consequently, an excess of gravitational potential energy resulted in extension ($\sigma_v > \sigma_H$) during Early Miocene basin formation. By the time topography and related crustal thickness variation relaxed (Middle Miocene), the stress field had rotated and the minimum horizontal stress axes (σ_h) became perpendicular

* Corresponding author. Institute of Geography and Earth Sciences, Eötvös Loránd University, Pázmány P. s. 1/C, 1117 Budapest, Hungary.
E-mail address: bada@ludens.elte.hu (G. Bada).
✠ Dr. Windhoffer has passed away.

0040-1951/$ - see front matter © 2005 Elsevier B.V. All rights reserved.
doi:10.1016/j.tecto.2004.10.019

to the main strike of the thrusts. The high topography and the rotation of σ_h could induce nearly pure extension (dip-slip faulting) along the pre-existing low-angle thrusts. On the contrary, the Derecske trough was situated near the Carpathian subduction belt, with lower crustal thickness and no pronounced topography. This resulted in much lower σ_v value than in the Danube basin. Moreover, the proximity of the retreating subduction slab provided low values of σ_h and the oblique orientation of the paleostress fields with respect to the master faults of the trough. This led to the dominance of strike-slip faulting in combination with extension and basin subsidence (transtension).
© 2005 Elsevier B.V. All rights reserved.

Keywords: Fault reactivation; Basin formation; Pannonian basin; Analogue and numerical modelling

1. Introduction

The Pannonian basin is characterised by a polyphase deformation history with a sequence of distinct structural episodes. Due to the convergence between the Adriatic and European plates, Cretaceous to Early Miocene basin evolution was taking place in a compressional stress regime, which had a major impact on the architecture of the basement units (e.g. Tari et al., 1993; Csontos and Nagymarosy, 1998; Fodor et al., 1999). Several thrusts, reverse fault systems, transpressional features and flexural basins were formed as a result of intense shortening. There is a general agreement that these structures, as pre-existing weakness zones, played a crucial role in subsequent tectonic phases such as the formation and then the deformation (late-stage inversion) of the Pannonian basin system (Horváth, 1993; Tari et al., 1999). A rapid and dramatic change of boundary conditions and, thus, tectonic style in the Early Miocene led to the formation of the Pannonian basin in the area of the Carpathian embayment. Consequently, the relatively stable Palaeogene to Early Miocene assembly of continental blocks at the axial zone of Adria–Europe convergence was completely disintegrated. These units experienced significant amount of stretching, block rotation and translation. Extension was concentrated in several local depressions that were connected to each other and to regions of coeval shortening in the Carpathian arc by numerous sets of conjugate strike-slip faults (Fig. 1). Elevated basement blocks separated deep sub-basins where thickness of the Neogene–Quaternary strata locally reaches 7–8 km. Such irregular basement morphology is mainly the result of strain localisation along pre-existing crustal weakness zones, mainly thrusts, inherited from the preceding phases of thrusting and nappe stacking.

There is a general agreement that lithospheric memory had a great influence on the mechanics of basin evolution in the form of reactivation of pre-existing weakness zones in the Pannonian lithosphere (e.g. Cloetingh and Lankreijer, 2001). Particularly, compressional structures played a crucial role during both the formation and the inversion of the basin system (cf. Horváth, 1993). However, the style, the kinematics as well as the temporal and spatial pattern of thrust fault reactivation have long been a matter of debate. Horváth and Royden (1981) emphasised the dominance of Miocene strike-slip faulting and, through this, the transtensional origin of the Pannonian basin as a whole. In contrast, Tari et al. (1992, 1999) argued for a dominantly pure extensional origin of the basin system with occasional transfer faults separating areas of differential extension. In these models, lithospheric extension and basin subsidence were initiated by the formation of metamorphic core complexes, where major part of the deformation was facilitated by low-angle normal faults that acted as reactivated older thrusts or nappe boundaries. Structural data, however, suggest that the dominant tectonic style strongly varied across the Pannonian basin and a uniform model of fault reactivation cannot be applied to the system. Certain sub-basins in the Pannonian basin are indeed of pure extensional origin (Tari, 1996; Tari et al., 1999), whereas others show clear pull-apart (transtensional) features (Horváth and Royden, 1981; Bergerat, 1989; Horváth, 1993; Csontos, 1995; Fodor et al., 1999).

Whereas the importance of extensional reactivation of Alpine thrust faults in the Pannonian region is well documented and, thus, generally accepted, the mechanical principles of these processes are not yet well understood. There are major mechanical problems with the reactivation of former thrusts or, more generally, reverse faults in an extensional stress regime (e.g. Sibson, 1985). It is well known in structural geology, and also confirmed by simple geomechanical considerations, that thrusts tend to be rather flat with a typical dip angle range of ca. 25–35°. On the contrary, normal faults are much steeper, mainly with dip angles of about 55–65° (e.g. Jaeger and Cook, 1976). Given this fundamental difference, the principle question arises: under what circumstances can reverse faults reactivate as normal faults? Ivins et al. (1990), for example, noted that "field observations of continental extensional faults are not predicted by the classical isotropic Mohr–Coulomb–Anderson theory". They suggested either en-

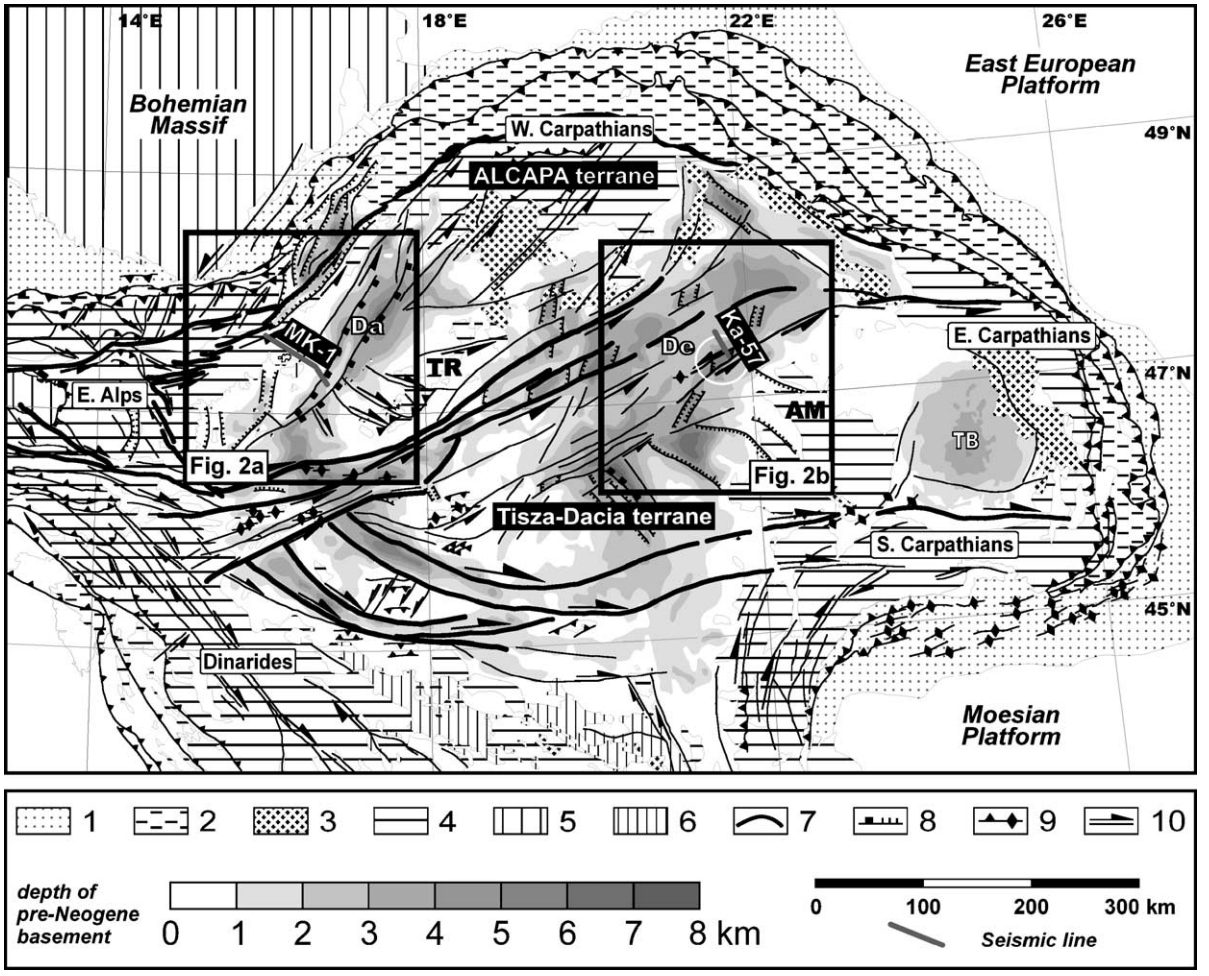

Fig. 1. Depth of pre-Neogene basement in the Pannonian basin system (after Horváth and Royden, 1981) and the related late Neogene structural pattern (after Horváth, 1993). Inserts indicate the broad location of the two study areas that are the Danube basin in the west (see Fig. 2a) and the Derecske trough in the east (see Fig. 2b). (1) Foreland (molasse) basins; (2) flysch nappes; (3) Neogene vulcanites; (4) pre-Tertiary units on the surface; (5) Variscan basement of the European plate; (6) Vardar ophiolites; (7) Pieniny Klippen Belt; (8) low-angle normal and normal fault; (9) thrust, anticline; (10) strike-slip fault. Heavy fault lines mark the diffuse boundaries of the main tectonic domains of Miocene paleogeographic reconstructions, i.e. the ALCAPA and Tisza-Dacia units in the north and south, respectively. The location of seismic profiles MK-1 and Ka-57 is indicated by heavy lines. AM: Apuseni Mts.; Da: Danube basin; De: Derecske trough; TB: Transylvanian basin; TR: Transdanubian Range.

hanced fluid pore pressure or low frictional strength for the reactivation of shallow dipping thrusts. Sibson (2000) also argued for the critical importance of fluid involvement to the frictional mechanics of fault reactivation under tension. Alternatively, transtension rather than dip slip is a viable mechanism, provided that the frictional parameters and, moreover, the style and orientation of the stress field relative to the fault are favourable (e.g. Ranalli, 2000).

The complex interplay between extensional structures and the underlying basement fabric has long been the subject of tectonic investigations. The key parameters controlling the reactivation potential of fracture zones are the fault geometry (dip angle, strike and shape), the mechanical parameters of the fault surface as well as the deforming medium (frictional coefficient, cohesion), the pore fluid pressure and the stress field (orientation and magnitude of principle stresses). With the aid of a series of analogue and numerical models, the role of four of these factors is addressed in this paper. We investigate the importance of (a) the dip angle and (b) frictional strength of the fault, (c) its orientation relative to the largest stress, and (d) the shape of the differential stress ellipsoid in both cases of extensional and strike-slip type stress field. The principle objective of the study was to simulate and analyse the reactivation mechanism of pre-existing basement faults (thrusts), and its relation to the formation of the Pannonian basin

system. We do so to provide mechanically plausible explanation for the observed deformation pattern and, in addition, to give further constraints on the dynamics and kinematics of extensional basin formation in an overall compressional setting of the Alpine orogenic system. The novelty of our investigation is the joint utilization of analogue and numerical modelling techniques in order to obtain reliable fault behaviour predictions. It should be realised that both the results of the sandbox experiments and numerical modelling need careful interpretation. In analogue modelling, by its nature, we work with very low stress values (actually with tensional stresses), and in this range the shape of the Coulomb–Griffith failure envelope is parabolic. Consequently, the internal friction angle (β) is variable. Therefore, the modelling results are very sensitive to small stress variations. In the case of numerical modelling, the obtained results also need caution, since reactivation depends on many different factors and the approach used in this paper is relatively simple.

The paper first presents a brief summary on the main tectonic features of the Pannonian basin with a special emphasis on the extensional Danube basin in the west and the pull-apart Derecske trough in the east. Then the basic assumptions and the setup of the analogue and numerical models are described, followed by the presentation of the modelling results. Finally, these results are discussed in the light of the tectonic history of the Pannonian basin with a special emphasis on the mechanics of basin formation and syn-rift basin evolution during Early to Middle Miocene times.

2. Geological setting: repeated tectonic reactivation in the Pannonian basin

The formation of the Pannonian basin system to a large extent was initiated and controlled by the process of gravitational collapse of overthickened lithospheric wedges that led to their lateral extrusion from the Alpine convergence zone towards the unconstrained Carpathian embayment (e.g. Ratschbacher et al., 1991; Horváth, 1993; Horváth et al., in press). Consequently, the relatively stable Palaeogene to Early Miocene assembly of structural domains, which makes up the basement of the Pannonian basin, was disintegrated and experienced significant amount of stretching and eastward body translation (Balla, 1984; Kováč et al., 1994; Csontos, 1995; Fodor et al., 1999). This plate-scale process, in combination with the internal deformation of tectonic units, resulted in the rifting of the Pannonian basin coeval with the eastward tectonic transport of the flysch nappe system in the Carpathian arc. Crustal wedges bounded by conjugate sets of strike-slip faults, i.e. sinistral and dextral in the north and south, respectively, were extruding and stretched in orogen-parallel direction to the east–northeast (Fig. 1). This process was coeval with further shortening in the central zone of the Eastern Alps, rapid exhumation of the lower tectonic units of the Alpine nappe stack (Penninicum) and, eventually, the formation of several metamorphic core complexes during Early to Middle Miocene times (Tari et al., 1999).

The architecture of the basement of the Pannonian basin reflects a polyphase tectonic evolution. The pre-rift lithospheric structure was formed during Cretaceous through Palaeogene times resulting in a complex system of nappe piles and compressional features. The Pannonian basin has been an area of pronounced lithospheric weakness after this compressional event, explaining the high level of strain rate. Miocene rifting of the basin system was strongly controlled by the inherent weakness of its basement in terms of bulk lithospheric strength (Lankreijer et al., 1999). On the other hand, the presence of upper crustal inhomogeneities, in the form of pre-existing shear zones and fault systems, appears to have had a first-order influence on the style of deformation and syn-rift basin geometry.

For the purpose of this study, two areas have been selected to demonstrate different fault reactivation mechanisms and kinematics, and related deformation style within the Pannonian basin system (Figs. 1 and 2, after Csontos and Vörös, 2004). The Danube basin in the west is located at the foothills of the Eastern Alps, while the Derecske trough is situated further to the east at the contact zone between the Pannonian basin and the Apuseni Mts. The comparison of Figs. 1 and 2 strongly suggests that in both cases the location and geometry of these local depressions are mainly determined by the presence of a set of major thrusts and nappe boundaries between the principle basement units. Basin formation and basement subsidence during the syn-rift phase (Early and Middle Miocene, sensu Royden et al., 1983) took place mainly along the reactivated segments of these shear zones either in a pure extensional (Danube basin) or in a transtensional or pull-apart (Derecske trough) manner. Below, we describe their structural features and highlight some of the main similarities and differences with the aid of two representative seismic reflection profiles across each of these two sub-basins.

2.1. Danube basin

The Danube basin is situated in the ALCAPA terrane and is superimposed on the compressional Alpine realm

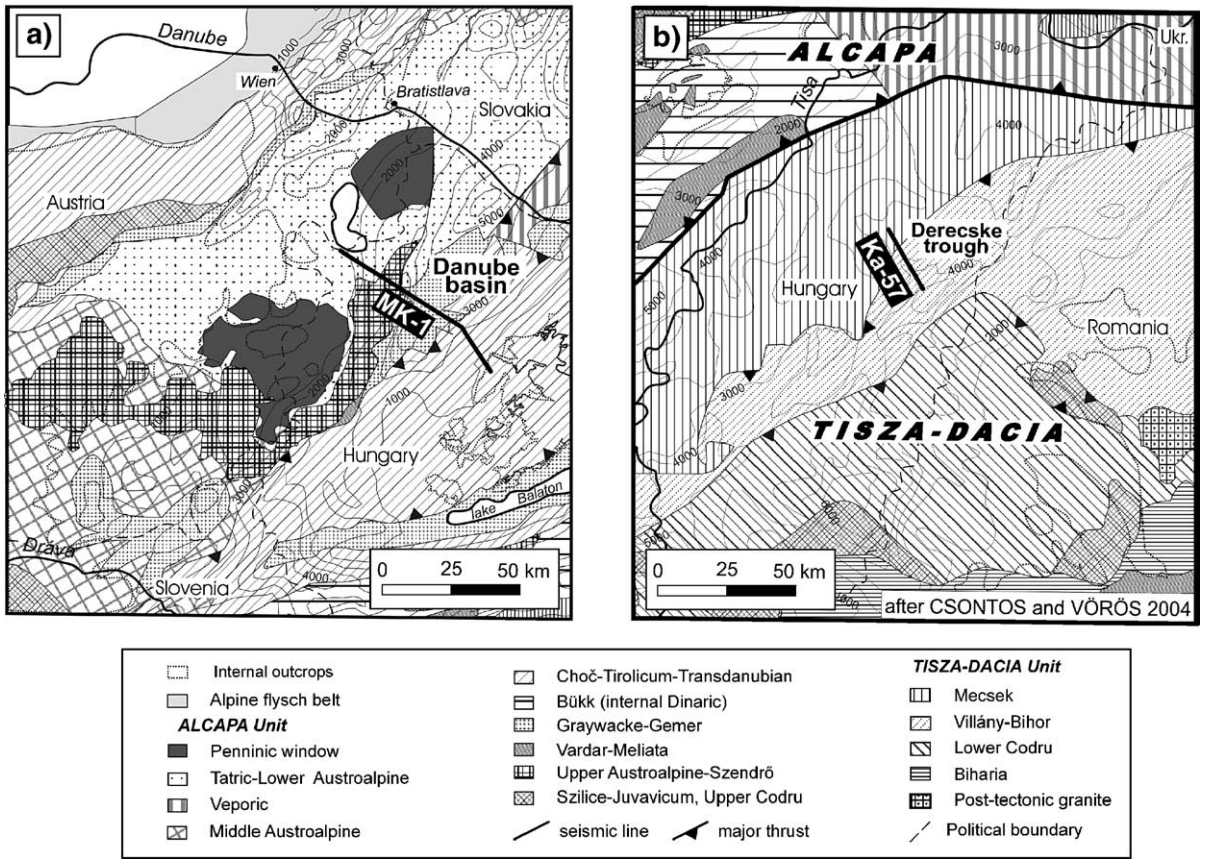

Fig. 2. Structural build-up of the pre-Neogene basement units in the area of (a) the Danube basin and (b) the Derecske trough (after Csontos and Vörös, 2004). Both basins are located on top of several Alpine nappe sheets in the ALCAPA and the Tisza-Dacia units, respectively. The related thrusts were reactivated during Miocene times facilitating large-scale crustal extension in the Pannonian basin system. The location of seismic profiles MK-1 and Ka-57 is indicated by heavy grey lines.

(Figs. 1 and 2). The basin was formed in an extensional corridor on top of the contact zone between nappe slices of Alpine origin (cf. Tari, 1994). Nappe emplacement took place during Cretaceous times resulting in the formation of several regional thrust faults with mainly NE–SW strike. NW directed tectonic transport emplaced (from bottom to top) Penninic, and Lower, Middle and Upper Austroalpine units on top of each other. These units are exposed in the Eastern Alps, whereas in the Danube basin they can be studied by means of reflection seismic sections and drill holes. The principle structural features of the basement units and the stratigraphic pattern of the basin fill (Tari, 1994) are shown on the line interpretation of profile MK-1 (Ádám et al., 1984) (Fig. 3). Basin formation was to a great extent initiated and controlled by the partial reactivation of major thrust planes as low-angle normal faults during the Miocene. The dominance of normal faulting and the lack of strike-slip faults are noteworthy and suggest the primarily extensional origin of the Danube basin (Tari, 1994).

Tari (1996) suggested two different ways of the reactivation pattern: (1) thrust planes are reactivated as normal faults over their entire length and (2) newly formed and steeply dipping normal faults sole out at depth in extensionally reactivated detachment levels. The author argued for the dominance of the second mode. Simple mechanical considerations, at least to a first approximation, would suggest that this slippage is hardly possible at such a low dip angle in an extensional stress regime. The flat-ramp-flat geometry of typical nappe contacts, however, may allow the steeper thrust segments (ramps) to reactivate. Fig. 3 reveals that only the steeper parts (min. 30–40° dip angle) of the thrust system show normal offset. On the other hand, flat thrust segments display no signs of Miocene reactivation, a feature recognised from geometry of the former flat-ramp-flat structures. The interplay between pre-existing compressional structures in the basement of the Danube basin and subsequent low-angle normal faulting is very complex. Since the style and amount of

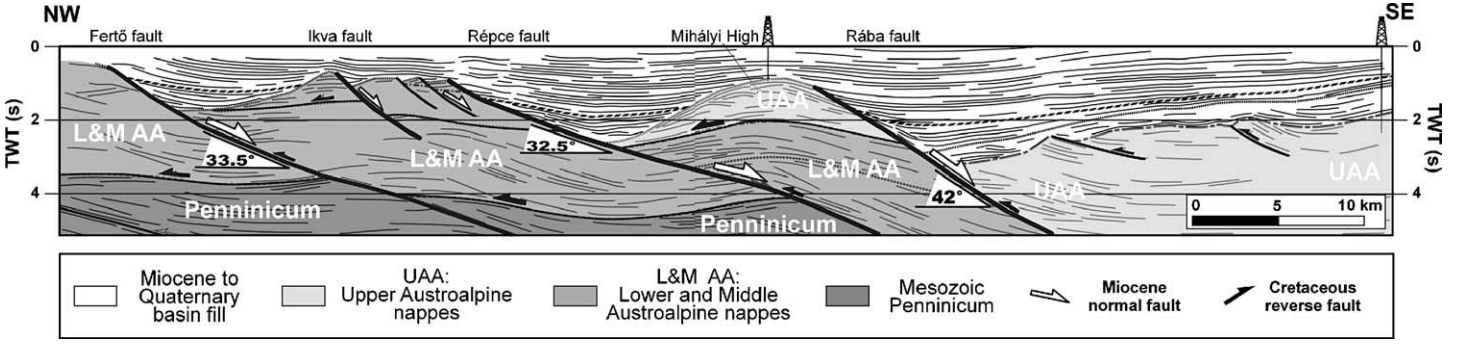

Fig. 3. Line-drawing interpretation of MK-1 deep seismic reflection profile across the Danube basin (after Tari, 1996). Heavy black lines mark reactivated Alpine (Cretaceous) thrust ramps, whereas the flat segments of the thrust planes denoted by thinner lines show no clear indication of Miocene reactivation. Numbers in white triangles refer to the average dip of the reactivated faults derived from depth converted version of the profile. For location, see Figs. 1 and 2a.

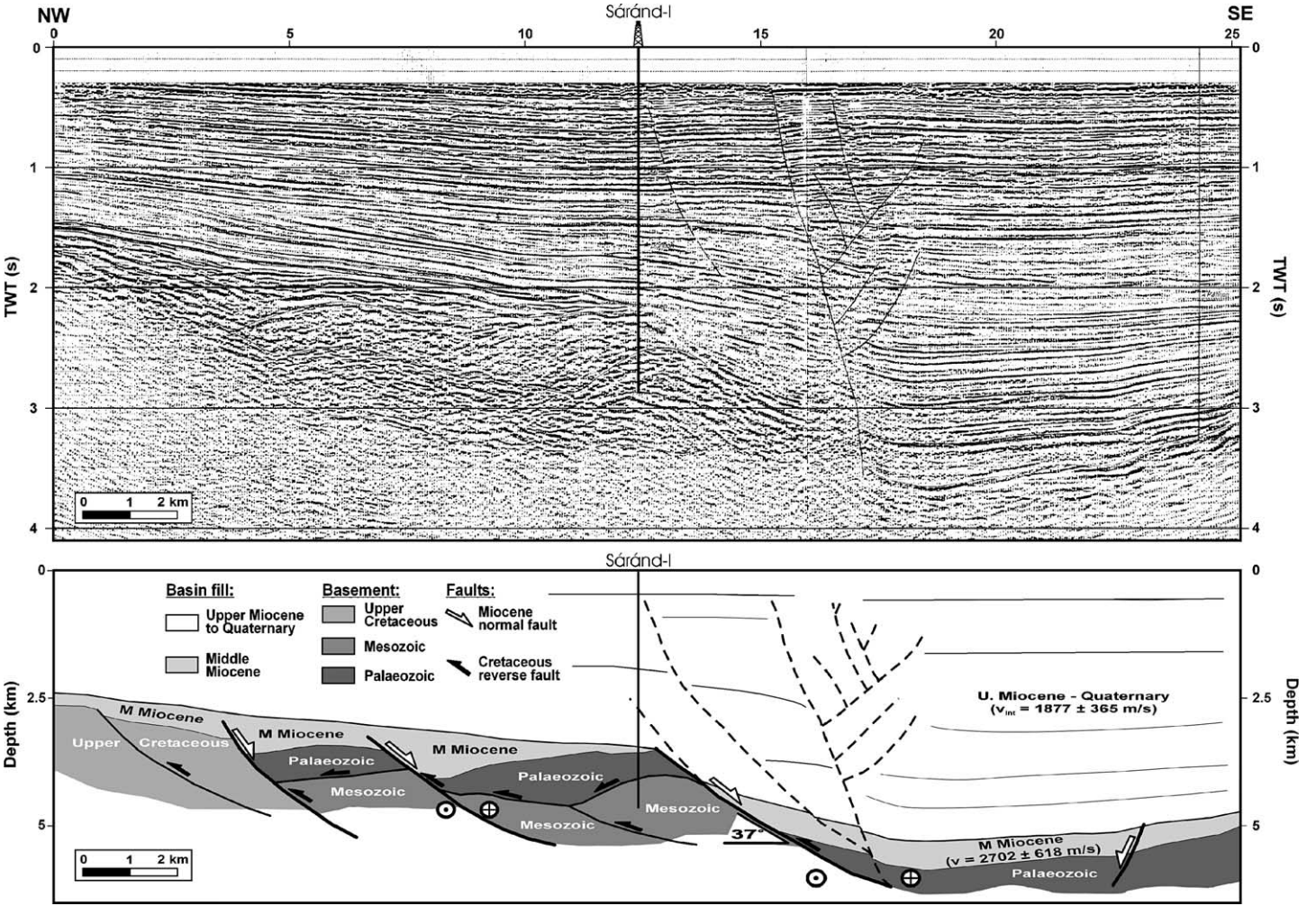

Fig. 4. Reflection seismic profile from the Derecske trough in the eastern part of the Pannonian basin (modified after Horváth and Rumpler, 1984) and its structural interpretation. Heavy black lines mark reactivated Alpine (Cretaceous) thrust ramps, whereas the flat segments of the thrust planes denoted by thinner lines show no clear indication of Miocene reactivation. This reactivation eventually led to typical half-graben basin architecture and to tilting of the basement blocks. The strike-slip component of the main normal faults has been derived from mapping the whole Derecske basin using a set of additional seismic profiles and borehole data. Dashed lines show fault segments of a negative flower structure formed during subsequent Quaternary strike-slip reactivation of Miocene extensional structures. Number in white triangle refers to the average dip of the reactivated fault derived from depth converted version of the profile. The seismic interval velocities (v^{int}) used for the depth conversion are indicated. For location, see Figs. 1 and 2a.

continental extension was mainly governed by this interaction, tectonic modelling was required to further explore the nature of fault reactivation mechanics.

2.2. Derecske trough

The Derecske trough is located in the Tisza-Dacia terrane (Fig. 1). The pre-rift structural build-up is quite similar to that of the Danube basin: its basement is made up of NW verging nappe slices of the Mecsek and Villány-Bihar units (Fig. 2). Fig. 4 presents a characteristic seismic profile transecting the central part of the Derecske trough (after Horváth and Rumpler, 1984).

The interpretation of the section follows an approximate depth scale, without vertical exaggeration. Velocity values for the depth conversion have been obtained from seismo-acoustic measurements. Conversion from the time to the depth domain contains approximately 6% error, which means $\pm 4^{\circ}$ error for the dip angles of the thrust faults.

Several major thrusts and reverse faults can be identified emplacing Palaeozoic strata on top of Mesozoic rocks. As in the case of the Danube basin, the flat-ramp-flat geometry of the thrusts has a major influence on their subsequent reactivation behaviour. While the flat segments of the thrusts remained mainly inactive, the steeper parts reactivated during the formation and syn-rift phase of the Derecske trough in the early and middle Miocene. Reactivation seems to have occurred only when the dip angle of the faults reached a threshold of ca. 35°, similar to the values of the Danube basin. Interestingly enough, the seismic profile shows a negative flower structure crosscutting the whole Upper Miocene to Quaternary basin fill, which roots in the large normal fault located in the middle part of the section. This indicates repeated tectonic reactivation with a first phase of Cretaceous thrusting, a second phase of Miocene transtension and finally Quaternary to present-day strike-slip faulting.

Besides all the similarities, the tectonic style of the Derecske and Danube basins exhibits important differences. As described above, the Danube basin is characterised by pure extension and mainly normal (dip-slip) faulting. The Derecske trough, however, evolved under transtension that led to the formation of a pull-apart basin as evidenced by the rhomboid shape of the basin and the presence of a set of strike-slip faults at the basin edges (Fig. 1; Horváth and Rumpler, 1984). This striking difference is difficult to reconcile with the basement architecture as it appears to be very similar in both cases. However, differences in the mechanical parameters of the thrusts or in the confining paleostress fields (Bada, 1999; Fodor et al., 1999) might provide plausible explanations. To test these scenarios, a parameter analysis has been carried out by means of analogue and numerical modelling techniques. First, we describe briefly the analogue, then the numerical modelling and their results, and we will conclude with a discussion of the obtained modelling results.

3. Analogue modelling of thrust fault reactivation

With the aid of the following analogue experiments, we aimed to examine thrust fault reactivation pattern often observed on seismic profiles in the Pannonian basin system. Two main different types of setup were applied in these experiments: (a) reactivation in pure normal faulting and (b) reactivation in transtension, i.e. normal faulting with considerable strike-slip component. At first, we introduce the theoretical background of analogue modelling, which is followed by the description of the obtained modelling results.

3.1. Model setup

Analogue (sandbox) modelling is a powerful tool to simulate deformation processes in laboratory. The basic material for the experiments is sand. Dry quartz sand simulates the brittle behaviour of rocks, such as sandstone or limestone. The sand deforms along narrow (shear) zones without creeping. This means that the emergent structures in the sand are time-independent to a certain limit and, therefore, it can easily mimic geological processes. In fact, very fast movements could induce an inertia effect; however, the used strain rates are far less than this limit. Silicone putty is used to simulate ductile behaviour of rocks like (overpressured) shale or salt. For the experiments, North Sea sand has been used. The density is 1600 kg/m^3 when sieved; its frictional coefficient is 0.52–0.84, while its cohesion is 1814 Pa when moistened. The content of the sand is mainly quartz with subordinate micas and other minerals. The pre-existing faults were formed by cutting the sand with a thin string after making it wet.

The scaling problem of analogue modelling was discussed by Hubbert (1937). The vertical stress from the overburden in the geological prototype is:

$$\sigma_p = \rho_p \cdot g_p \cdot h_p \quad (1)$$

while in the model:

$$\sigma_m = \rho_m \cdot g_m \cdot h_m \quad (2)$$

where ρ is the density of the given material, h is the depth and g is the gravitational acceleration. The ratio of these two stresses is:

$$\sigma_m/\sigma_p = \rho_m \cdot g_m \cdot h_m/\rho_p \cdot g_p \cdot h_p h_m/h_p \quad (3)$$

since the ratio of the densities is close to one. It means that the stresses are scaled by approximately the same ratio as the length (depth). The frictional behaviour provides us another scaling factor. In the model, as well as in the geological prototype, faulting happens according to the Coulomb's criterion:

$$\sigma_s \geq C_o + \mu \cdot \sigma_n \quad (4)$$

where σ_s and σ_n are the shear and normal stresses, respectively, while C_o is the cohesion and μ is the tangent of the internal friction angle of the deforming medium. It means that the cohesive strength has to be scaled down by the same factor as the stresses and length. Scaling values for sandbox modelling is given by the fact that typically a 10-cm-thick layer cake in the model corresponds to 1- to 10-km-thick structure in reality.

The sedimentary overburden is moderately cohesive material and it has a frictional plastic behaviour at the time of faulting. Given these conditions, we can appropriately carry out modelling with dry sand. However, wetting the sand with approximately 10% mass percentage of the dry material significantly increases its cohesion. Therefore, it becomes suitable for modelling underlying, relatively stronger rocks (Jaeger and Cook, 1976; van Mechelen et al., 2003). Attraction between dry sand grains is so small that it is impossible to measure it properly. By wetting the sand, we add a film of water around the sand grains without filling the pore space between them. On the grain-to-grain contact points, water bridges form. The water bridges provide the strength for the sand pack, which comes from the surface tension of the water. There should be no water in the pores, because that creates pore pressure and will immediately reduces the strength of the sand dramatically and eventually results in liquefaction. Making the sand wet does not considerably change the internal friction (van Mechelen et al., 2003).

Table 1 shows some average values of cohesion and frictional coefficient. As one can see, the scaling factor derived from the vertical stress of the overburden (10^5) is valid for cohesion as well. In analogue modelling, moistening the sand increases its cohesion. In case when these high cohesion values are converted into "real" ones, using the above-mentioned scaling factor, they well exceed the maximum values of strong rocks found in nature (e.g. marble). Therefore, the experienced range of reactivation angles in sandbox experiments is larger than in reality. In other words, the obtained least dip angle of reactivation during sandbox modelling is a conservative estimate for reactivation angle in nature.

Table 1
Table of cohesion and frictional coefficient values for different materials

	Sandstone	Marble	Dry sand	Wet sand
Cohesion (Pa)	$2.8 \cdot 10^{5}$[a]	$1.1 \cdot 10^{6}$[a]	23[b]	1814[b]
Frictional coefficient	0.51[a]	0.75[a]	0.85[b]	0.52[b]

[a] Jaeger and Cook (1976).
[b] van Mechelen et al. (2003).

The advantage of using wet sand in these kinds of reactivation models can be well represented in a Mohr-diagram (Fig. 5). When pulling a sand (or rock) block, σ_3 decreases and, accordingly, the diameter of the Mohr circle increases and can reach the failure envelope of dry sand. Consequently, a new normal fault may be initiated while the pre-existing fault remains stable (stage 2). Further decrease of σ_3 in case of dry sand could lead to generation of a set of normal faults with a range of dip angle and, most importantly, the initiation of reactivation of the pre-existing fault (stage 3). However, in case of wet sand the failure envelope is shifted upwards along the y-axis that is the cohesion increases and the internal strength remains approximately the same. Then fault reactivation seems to occur without forming normal faults (stage 4).

In order to test the reproducibility of the experiments, several of them were repeated twice or three times and similar results were obtained. All the experiments have been documented by digital photography.

3.2. Modelling results

Two significantly different modelling experiments were carried out in order to simulate the tectonic evolution of both the Danube and the Derecske basins. Firstly, pre-existing thrust faults have been reactivated in pure extension. During these experiments, the reactivation was examined as a function of the dip and the frictional properties of the pre-existing faults. The dip values used in these experiments reflect the situation observed on the seismic profile from the Danube basin (Fig. 3). The second part of the experiment series was the reactivation of pre-existing thrust faults in transtensional manner. In both cases, the thrust faults were planar. Using listric faults instead would decrease the possibility of reactivation on the curved parts of the fault with these modelling parameters.

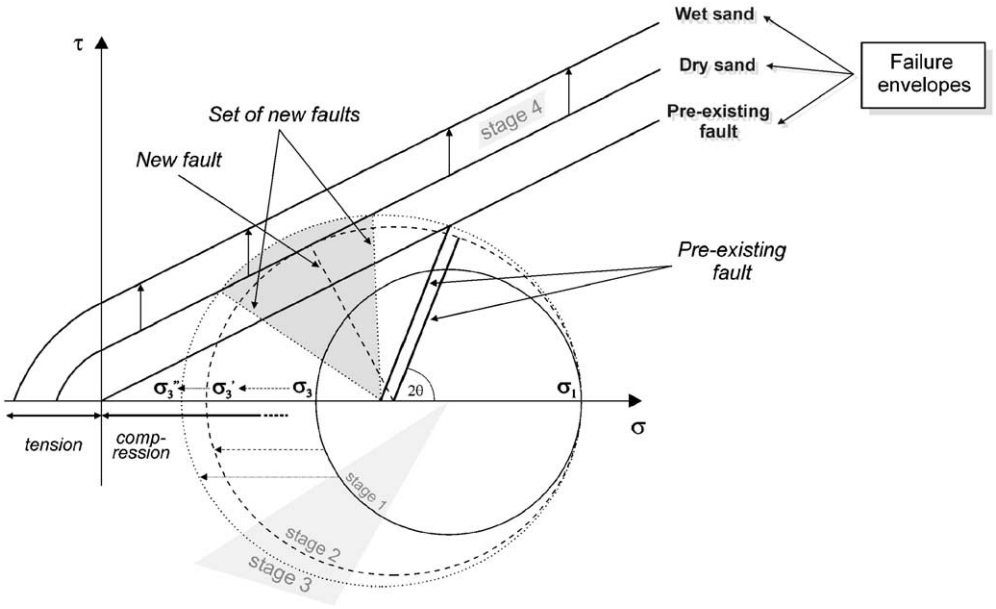

Fig. 5. Mohr-diagram showing failure envelopes for a pre-existing fracture, and for wet and dry sand. In the case of a stronger wet sand and applied extension (σ_3 decreases in magnitude), the Mohr circle can eventually touch the failure envelope of a properly oriented pre-existing fault. This fault thus is reactivated before a new fault may form.

Following the works of McClay and Massimo (2001) and Richard et al. (1995), the modelling aimed at the analysis of the strike and dip dependence of fault reactivation. The selected strike values represent the orientation of the fault with respect to the local stress field, whereas the dip angle is an average value that obtained from the seismic profiles (Fig. 4).

3.2.1. Thrust fault reactivation in pure extension

In these experiments, attempts were made to reactivate pre-existing thrust faults with different dip angle in pure extension. This was done by pulling the sand perpendicular to the strike of the pre-defined fault. The objective was to constrain the minimum dip angle of a fault plane on which reactivation can occur. Typical faulting angle of thrust faults is in the range of 25–35° (with respect to a horizontal plane), whereas normal faults are usually much steeper with typical dip angles between 55° and 65°. These values critically depend on the internal friction angle (ϕ) of the deforming medium. With the aid of the experiments, we analysed under what circumstances a low-angle thrust fault can be reactivated as a normal fault.

The setting of the experiments is shown in Fig. 6. The displacement rate of the backstop was 5.1 cm/h. The basement of the model was made up of a wooden plate and a silicone putty layer to avoid space problem as during reactivation the hanging wall block was subsiding. The faults rooted in the silicone putty layer in order to avoid the edge effects at the wooden plate.

3.2.1.1. Reactivation as a function of dip angle. The dip angle of the pre-existing fault changed from 60° down to 40° with an increment of 5° (Table 2). From 60° to 45°, the experiments showed common behaviour. In all these cases, reactivation occurred (Fig. 7, Photo 1). The exposed fault planes were crescent-shaped (Fig. 6). The total displacement of the backstop was kept constant at 8 mm in order to make a direct comparison between the fault displacement patterns in the different experiments. The 8 mm in our model correspond to 800 m in nature. The displacement along the reactivated thrust decreased with decreasing dip angle of the pre-existing fault. At dip angle of 40°, the attempt of reactivation failed. The hanging wall block simply rotated back while a fault gorge opened up (see insert in Fig. 6). We tried to avoid the rotation by using a double-long hanging wall block (Fig. 6) with 40° dip angle of the pre-existing fault, but the experiment failed again. These findings are in good agreement with fundamental theoretical considerations. We believe that this is not due to the intrinsic limitation of the model. In the circumstances that we have studied, exclusively in the brittle domain, movements on a low-angle plane (less than 45°) will not occur. Introducing silicone putty in order simulates a very low friction surface, can lower this angle but only to a limited degree.

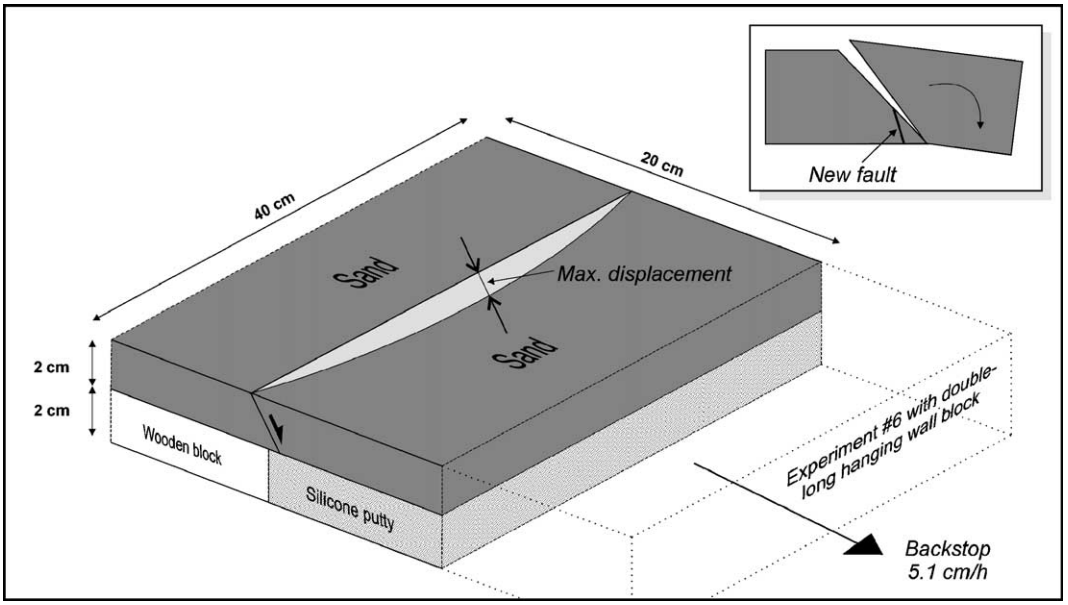

Fig. 6. Analogue model setup for experiments of fault reactivation in pure extension, i.e. with pulling direction parallel to dip of the pre-existing fracture. Insert shows the result of experiment #5.

The results of these experiments suggest that reactivation of a thrust fault with "normal" (i.e. not weak) frictional resistance and with a dip angle of ca. 30–35°, requires an increase of its dip angle prior to reactivation. This can be achieved by tilting the whole system, including the faults themselves. This process is very common in orogens such as the Alps, where the tectonic load of the overstacking nappe piles results in the thickening of the crust and isostatic uplift of the orogen. Differential uplift may eventually lead to a significant (>10°) tilt of the thrust system making them prone to subsequent extensional reactivation. Furthermore, it can also be assumed that during the development of a thrust sequence, the former ones can tilt due to the loading effect of the newly formed thrust lids, i.e. the original angle of the thrusts can become gradually steeper. However, measuring the real dip of the thrust faults on the depth converted seismic profiles, the Danube basin is characterised by dip angle values of 30–45° (Fig. 3), whereas in the Derecske trough these values are ca. 37° (Fig. 4). Therefore, other mechanisms have been sought to provide a more plausible fault reactivation model.

3.2.1.2. Reactivation as a function of frictional properties. In this series of experiments, the fault planes were made weaker by applying silicone putty on them. The dip angle of the pre-existing fault was 40° and 35° (Table 3). The geological analogy of a weak fault zone can be high pressure fluids on the fault plane.

Table 2
Summary of thrust fault reactivation analysis in pure extensional manner as a function of the dip angle of the pre-existing fault, using analogue modelling

Extension					
Exp. no.	Dip angle	Strike-angle	Reactivation	Note	
				Displacement	Fault habitat
#1	60°	0°	+	6 mm	Sand on sand
#2	55°	0°	+	5.5 mm	Sand on sand
#3	50°	0°	+	5 mm	Sand on sand
#4	45°	0°	+	3 mm	Sand on sand
#5	40°	0°	–	–	Edge of the footwall broke
#6	40°	0°	–	–	The hanging wall is twice longer

The dip angles of the fault planes are with respect to the horizontal plane, while strike angles are measured between the maximum horizontal stress and the strike of the fault planes. Displacement values were measured at the middle part of the fault, where it was maximal. The overall length of the faults was 30 cm.

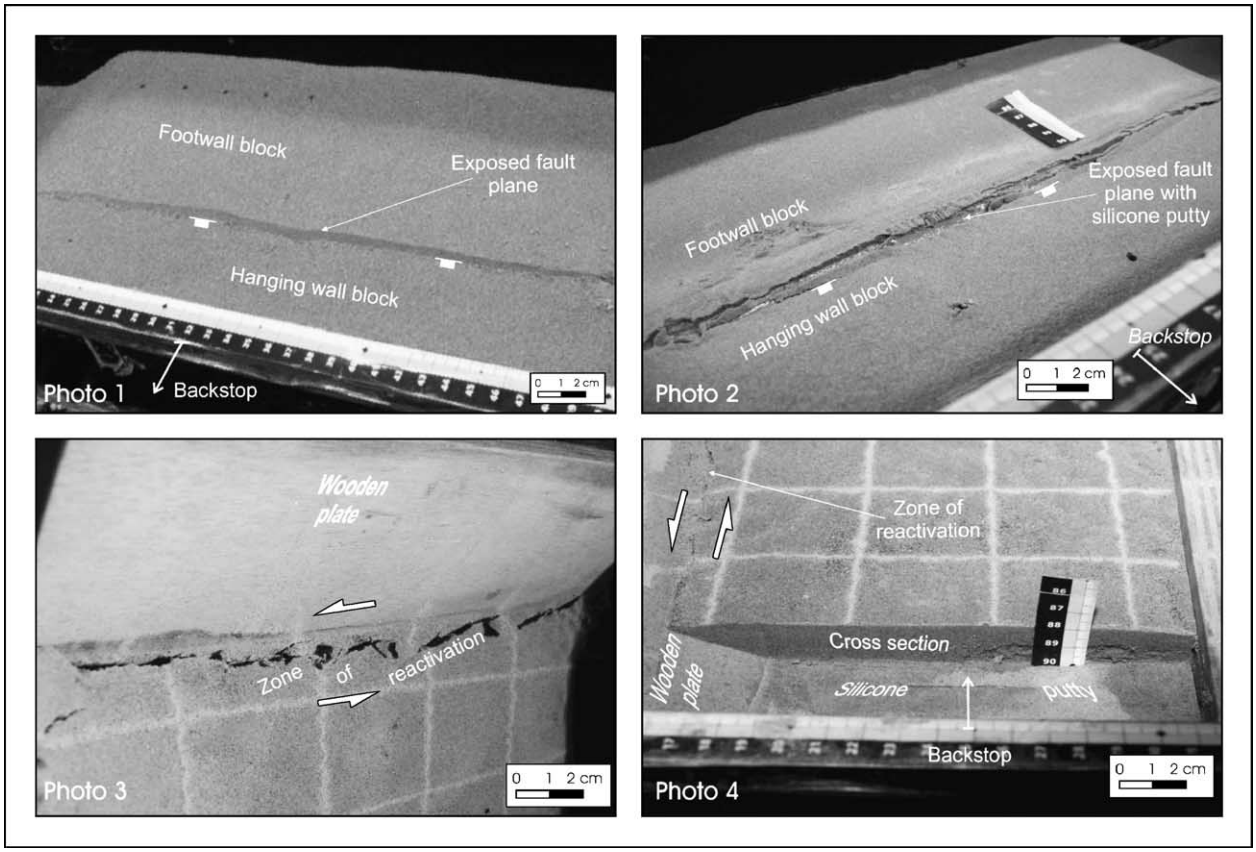

Fig. 7. Photos of typical reactivation features observed in the analogue (sandbox) models. Photos 1 and 2 show fault reactivation in pure extension with and without silicone putty on the fault planes, respectively. Photos 3 and 4 show reactivation of former thrust planes in oblique extension (transtension) also with and without silicone putty on the fault planes.

When overpressure can be maintained on low-angle fault plane (Sibson, 2000), reactivation in a normal faulting manner will be more likely than the formation of new faults.

We were able to reactivate the faults at the dip angle of 40° and 35° with 2 mm silicone putty on the fault planes (Fig. 7, Photo 2). On the other hand, 1 mm silicone was not enough to activate the 35° dip fault. A thinned silicone putty layer has higher friction and it has a drag-effect on the boundary between the sand and the putty that is the thinner the layer, the more the drag effect is observed. The deformation rate, which was used in the models is low enough for the silicone putty to be definitely in a very low-resistance deformation state, i.e. in the Newtonian viscous regime. This means that in our models a silicone putty surface effectively acts as a surface with very low (almost zero) frictional resistance. Although we did not quantify how weak a fault can be with 1 or 2 mm silicone putty on it, for the purpose of our study, the qualitative approach was sufficient. For comparison, an attempt has been made to reactivate a fault plane with a 40° dip angle in

Table 3
Summary of thrust fault reactivation analysis in pure extensional manner as a function of the frictional properties of the pre-existing fault, using analogue modelling

Extension				
Exp. no.	Dip angle	Strike-angle	Reactivation	Note
#7	40°	0°	+	2 mm silicone putty on the fault
#8	35°	0°	+	2 mm silicone putty on the fault
#9	35°	0°	–	1 mm silicone putty on the fault
#10	40°	0°	–	Dry sand

The fault planes were made weaker by using silicone putty on them.

dry sand but the experiment failed. In the last two cases, new faults were created with approximately 70° of dip angle in the hanging wall block. If we define α as an angle between σ_1 and the fault plane, than the tangent of internal friction angle ($\mu = \tan(\beta) = \tan(90^\circ - 2\alpha)$) of the sand is 1.19 under this low stress state. The reason for this is that the analogue experiments take place at very low stresses, which is a domain where β is highly variable. At tensile stresses and very low shear stress values, this angle is almost 90°. At higher angles, β gradually decreases until it stays at about 30° for sand. In summary, if the friction on fault plane is relatively low a low-angle thrust fault can be reactivated relatively easily even at lower dip angles (35–40°).

3.2.2. Thrust fault reactivation in transtension

The setting of these models differs from the previous ones in only one major aspect (Fig. 8). Transtension was produced in the model by *pushing* the hanging wall block away from the footwall block in an oblique manner. This means that the hanging wall block was under compression during the experiments. This way the sand becomes obviously stronger than in the extensional cases, therefore a wider range of reactivation can be expected.

At first, the strikes then the dips of the pre-defined faults were altered. The setting of these experiments is shown in Fig. 8. The opposite side of the backstop was kept free, while the opposite side of the fault plane was closed by a wooden block. The sand was glued on the wooden plate in order to simulate sand-to-sand friction along the fault. This way a surface is produced that is fixed in position with the same frictional coefficient as with the loose sand. Former observations show that the actual slip along this predetermined fault plane takes place a small distance away from the wooden plate (0.5 mm or less), just enough to enable some minor grain movements in the fault zone. The actual mechanical properties of the fault zone are therefore exactly the same as a fault in loose sand. The glued sand surface has its most important role that it determines the exact plane along which the shearing will take place. The sand was deposited on a silicone putty layer in order to evenly distribute the stress applied by the backstop throughout the model. The displacement rate of the backstop was again 5.1 cm/h.

3.2.2.1. Reactivation as a function of strike angle. The strike of the pre-existing fault changed from 30° down to 5°, while the dip angle was kept at a constant value of 37°. With this relatively wide range of strike angles, we intended to simulate the orientation of the far stress field (30°) on one hand, and the local stress deviation often observed in the Derecske basin (Windhoffer et al., 2003b). In almost all these cases, reactivation occurred (Table 4). However, the uppermost few millimetres of the sand usually remained stuck to the wooden plate, and in this manner new fault "systems" formed (Fig. 7 and 9, Photo 3). The angle of these new small faults *with respect to the pre-existing fault* (in top view) decreased through time during each experiment. The first population is formed at relatively high angle (30°). Then these faults were connected by fractures of lower strike angle in such a

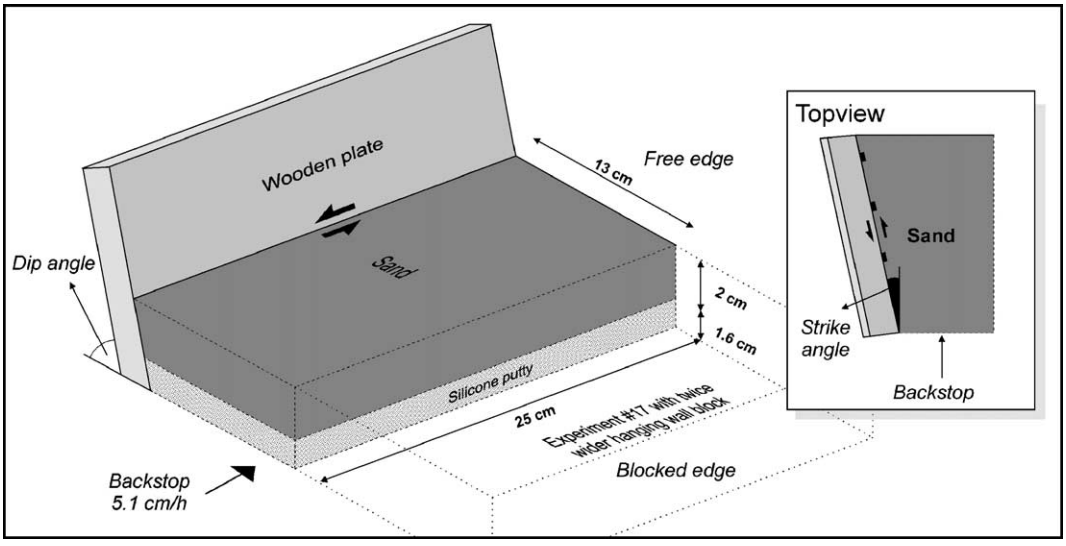

Fig. 8. Analogue model setup for experiments of fault reactivation in oblique extension (transtension). Insert shows the top view sketch of the experiments.

Table 4
Summary of thrust fault reactivation analysis in transtensional manner as a function of the strike angle of the pre-existing fault, using analogue modelling

Transtension				
Exp. no.	Dip angle	Strike-angle	Reactivation	Note
#11	37°	30°	+	Wet sand
#12	37°	20°	+	Small parts stuck to the wooden plate
#13	37°	12°	+	No sand glued on the fault, wet sand
#14	37°	12°	–	Dry sand
#15	37°	12°	+	Wet send
#16	37°	5°	–	Fault opens up
#17	37°	5°	+	Hanging wall is twice wider

The dip angle was kept constant 37° as it can be observed on the seismic profile of the Derecske basin (Fig. 4).

way that parts of these structures became inactive. Between the fault branches, small pop-ups or basin structures developed (Fig. 9, based on experiment #17).

The case of 12° strike angle was tested with dry sand (#14), wet sand (#15) and with no sand glued on the wooden plate (#13). The dry sand was not strong enough to bear the applied stress and a strike-slip system developed, rooting in the silicone putty–wooden plate contact zone. At 5° strike angle the experiment failed, the backstop simply opened up the whole sand pile. The experiments were repeated with a twice wider hanging wall block and reactivation occurred (see Fig. 8).

The interpretation of experiment #17 can be that this new fault zone is similar to the features described in the classical experiment of Tchalenko (Tchalenko, 1970). First, Riedel (R) faults develop and then P faults connect R faults eventually forming a continuous principle displacement zone (PDZ) with characteristic en-echelon geometry typical for many strike-slip fault zones.

3.2.2.2. Reactivation as a function of dip angle. The dip of the pre-existing fault changed from 35° down to 10° while the strike of the fault was kept constant at 5° with respect to the motion of the backstop (Table 5). The hanging wall was kept as wide as the last experiment of the former series.

In experiment #19 (30° dip, 5° of strike), obvious reactivation occurred. It is interesting to note that the lower half of the sand remained dry due to an inappropriate wetting of the sand. The only newly formed fault was rooting in the dry–wet contact zone, which later became inactive. As mentioned above, small parts of the sand usually remained stuck to the wooden plate. In experiment #21 (20° dip, 5° of strike), the wooden plate was totally covered by glued sand and reactivation occurred all along the fault plane (Fig. 7, Photo 4). With a dip angle of 10°, the attempt of reactivation failed (#22). Instead, as the dip of the pre-existing fault was too low, a new high-angle (with respect to the

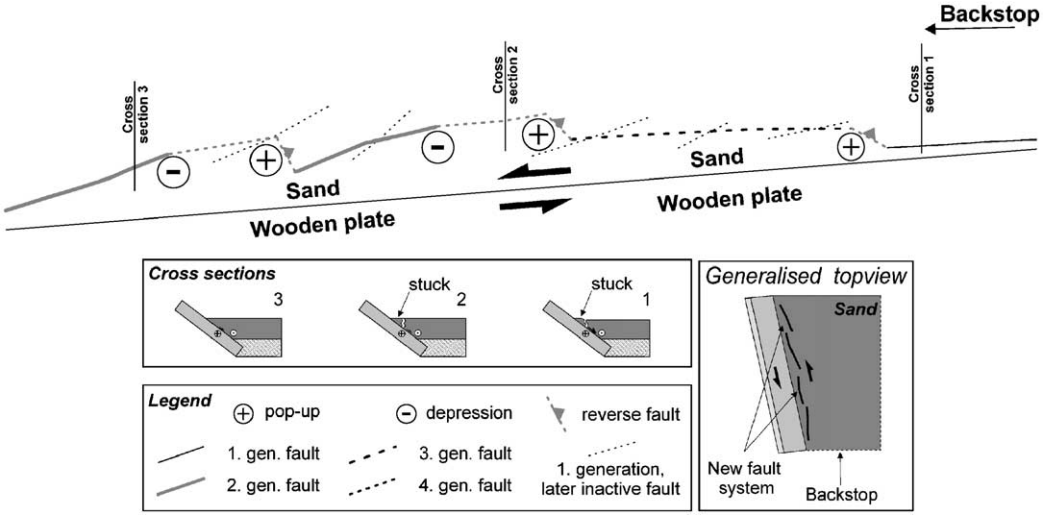

Fig. 9. Line-drawing results of analogue modelling showing the geometry and temporal sequence of a newly formed strike-slip fault system rooted in the pre-existing fracture at the contact between the wooden plate and the sand (experiment #17, top view). Selected cross sections show various features within the sand body. The generalised top view depicts a newly formed fault system of en-echelon geometry.

Table 5
Summary of thrust fault reactivation analysis in transtensional manner as a function of the dip angle of the pre-existing fault, using analogue modelling

Transtension				
Exp. no.	Dip angle	Strike-angle	Reactivation	Note
#18	35°	5°	+	Wet sand
#19	30°	5°	+	Lower part of the sand was dry, new fault rooted in the dry–wet contact zone
#20	20°	5°	Partly	Partial glue cover, partial reactivation
#21	20°	5°	+	Full glue cover, full reactivation
#22	10°	5°	–	New faults rooted in the silicone–wooden plate contact zone

The strike angle was kept constant 5°.

horizontal plane) fault zone was formed that rooted in the wooden plate–silicone putty contact and cut through the whole sand block.

As a major outcome, it can be concluded that even low-angle (20–35°) thrust faults can be reactivated in transtensional manner where the pre-existing fault is obliquely oriented with respect to the principal stress axes. Reactivation occurs with a relatively wide range of angles between the strike of the pre-existing fault and the direction of the minimum horizontal stress axis (σ_h).

4. Numerical modelling of thrust fault reactivation

Numerical modelling has been carried out to understand and further constrain thrust fault reactivation, and to cross-check the results of the sandbox experiments. Through this, we aimed at a deeper insight on fault behaviour and dynamics. The principle aim was to identify faults with low and high probability of slip. Two different types of models were run including the reactivation in pure extension (normal faulting) and in a strike-slip stress regime (transtension or transpression). First, we present the theoretical principles and setup of the numerical models, followed by the description of the modelling results.

4.1. Model setup

4.1.1. Theory of fault reactivation

In homogeneous and isotropic media (rocks), the stress field can be characterised by a relatively simple stress tensor. Knowing all the elements of this tensor, and the cohesion and internal friction angle of the observed rock volume in the brittle domain, one can predict the orientation of the fault plane, which may form as a result of the applied stress field (Anderson, 1951). However, rocks with pre-existing weakness zones can respond in a different manner to the stress field acting on the rock volume. Shear stress develops on the plane of weakness, and if this shear stress exceeds a certain limit slip occurs in the direction of maximum shear stress (Wallace, 1951). In order to confirm the former statement, we should take into account Wallace's (1951) and Bott's (1959) assumptions: (1) faults are planar and infinite, (2) displacement along the faults is small, (3) fault blocks are rigid and no block rotation occurs, (4) faults do not interact and (5) a single homogeneous stress field is acting in the model. This is a first-order approximation to describe fault reactivation. Using this method, one should neglect several factors, which influence the response of a given rock block to the applied stress field, such as fault interaction, fault block rotation, high strain rate and that in nature faults are finite.

The reactivation of pre-existing faults can be described in a similar way as in Eq. (4) (Jaeger and Cook, 1976):

$$|\sigma_s| \geq C_o + \mu_{slide} \cdot \sigma_n. \quad (5)$$

Neglecting the cohesion along a pre-existing fault (Sibson, 1974), Eq. (5) becomes simpler:

$$|\sigma_s| \geq \mu_{slide} \cdot \sigma_n, \text{ that is } \sigma_s/\sigma_n \geq \mu_{slide}. \quad (6)$$

Slip tendency (ST), as a quantitative measure for the reactivation potential, was defined by Morris et al. (1996) as the ratio of the shear and the normal stress along any given point on the fault surface:

$$\sigma_s/\sigma_n = \mathrm{ST}. \quad (7)$$

Comparing Eqs. (6) and (7), slip occurs when the absolute value of the slip tendency on the fault plane is larger than the frictional resistance at the same place, that is:

$$\mathrm{ST} \geq \mu_{slide}. \quad (8)$$

Whether slip indeed occurs is hard to predict as reactivation critically depends on the frictional characteristics of the surface of the fault. In fact, the actual frictional resistance of the fault is usually estimated or simply unknown. Therefore, it is necessary to emphasise

that the calculated slip tendency values will not give us a unique solution for fault reactivation. Nevertheless, higher slip tendency, which corresponds to lower frictional resistance (FR), certainly means higher slipping probability. If the ST value on a fault is lower than the lower limit of a reasonable range of slip thresholds, then one could reliably say that the given fault is most likely locked in that particular stress field. On the other hand, if the slip tendency is higher than the higher limit of the slip threshold, the fault can definitely be considered prone to reactivation (Wórum et al., 2004). This way the analysis of slip tendency provides useful constraints on the likelihood and style of fault reactivation.

As it was pointed out, the frictional coefficient (μ_{slide}) is a material property, thus mainly controlled by the rock type, and shows great variability. Accordingly, one can find a wide range of μ_{slide} values in the literature, connected to rocks in the nature, ranging from 0.3 to 0.8. During the analysis of the modelling results, we refer to a range of frictional coefficient values to compare them with slip tendency values. For convenience and practical considerations, the low-

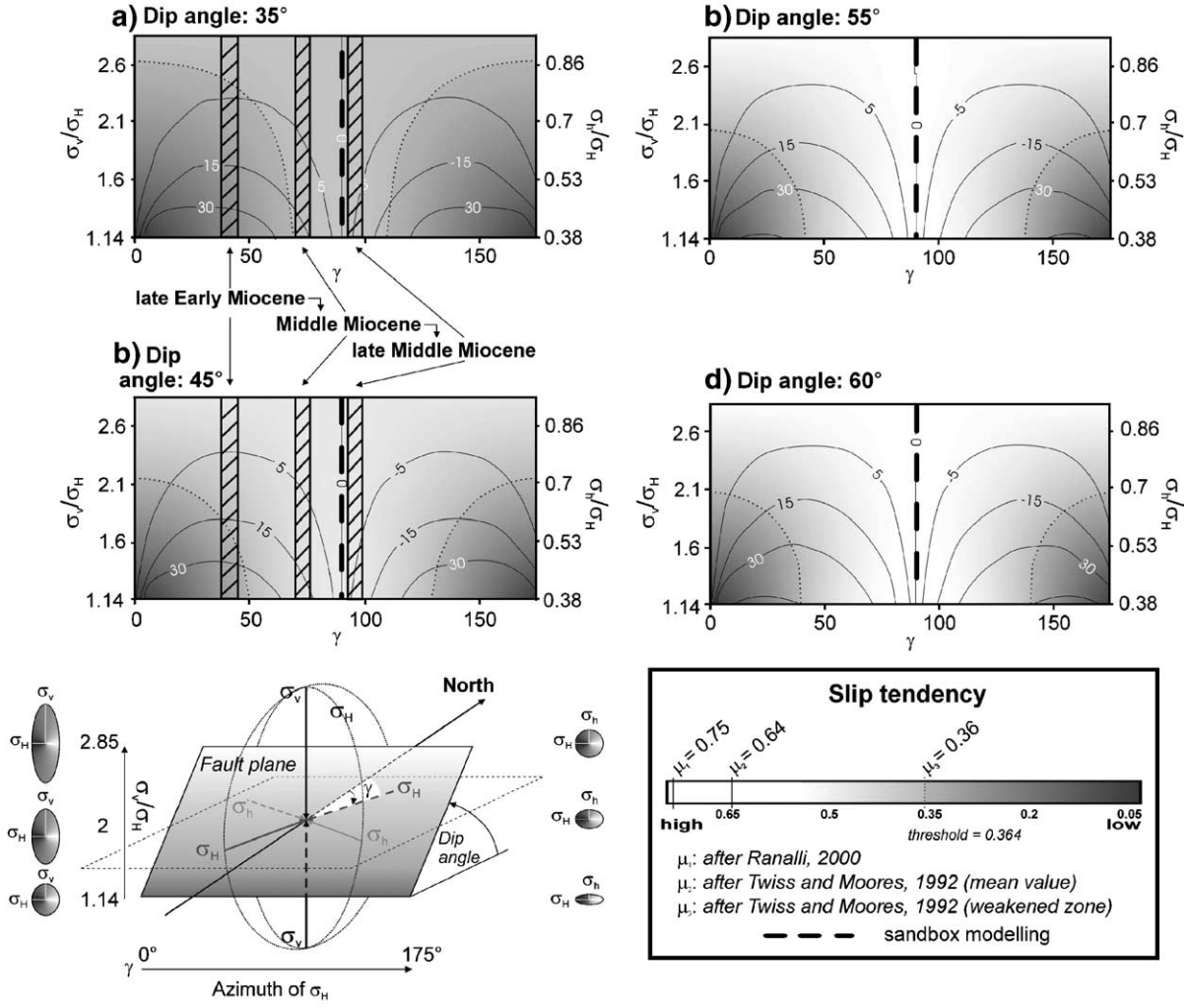

Fig. 10. Results of numerical modelling of fault reactivation in an extensional stress field ($\sigma_v > \sigma_H > \sigma_h$). For convenience, the fault is dipping to the south. The azimuth of the maximum horizontal stress direction ($0^\circ \le \gamma \le 175^\circ$) is on the horizontal axis, while the ratios of σ_v/σ_H and σ_h/σ_H are on the vertical axis. Reactivation pattern is analysed through seven steps as a function of dip angle of the fault. Greyscale colouring shows slip tendency values, dashed line indicate the selected threshold value of 0.364. Other frictional angle values taken from the literature are also shown in the legend. Contour lines indicate slip direction on the fault planes where 0°, 90° and -90° refer to normal, left lateral and right lateral faulting, respectively. Between these extremes, values of 0° to 90° and -90° to 0° indicate sinistral or dextral transtension, respectively. Heavy black lines mark the parameters of the sandbox experiments. Note that the figure is not symmetrical, since the horizontal scale is from 0° to 175°. Sketch in the lower left corner shows the spatial distribution of the fault plane and the stress ellipsoid. The small grey ellipsoids on both sides of the sketch represent stress ratios.

est threshold value has been set to 0.364 (Twiss and Moores, 1992) and is marked in Figs. 10, 11 and 12 by dashed lines.

4.1.2. Modelling procedure

A numerical code after Wórum et al. (2004) has been applied in this paper for simulating thrust fault

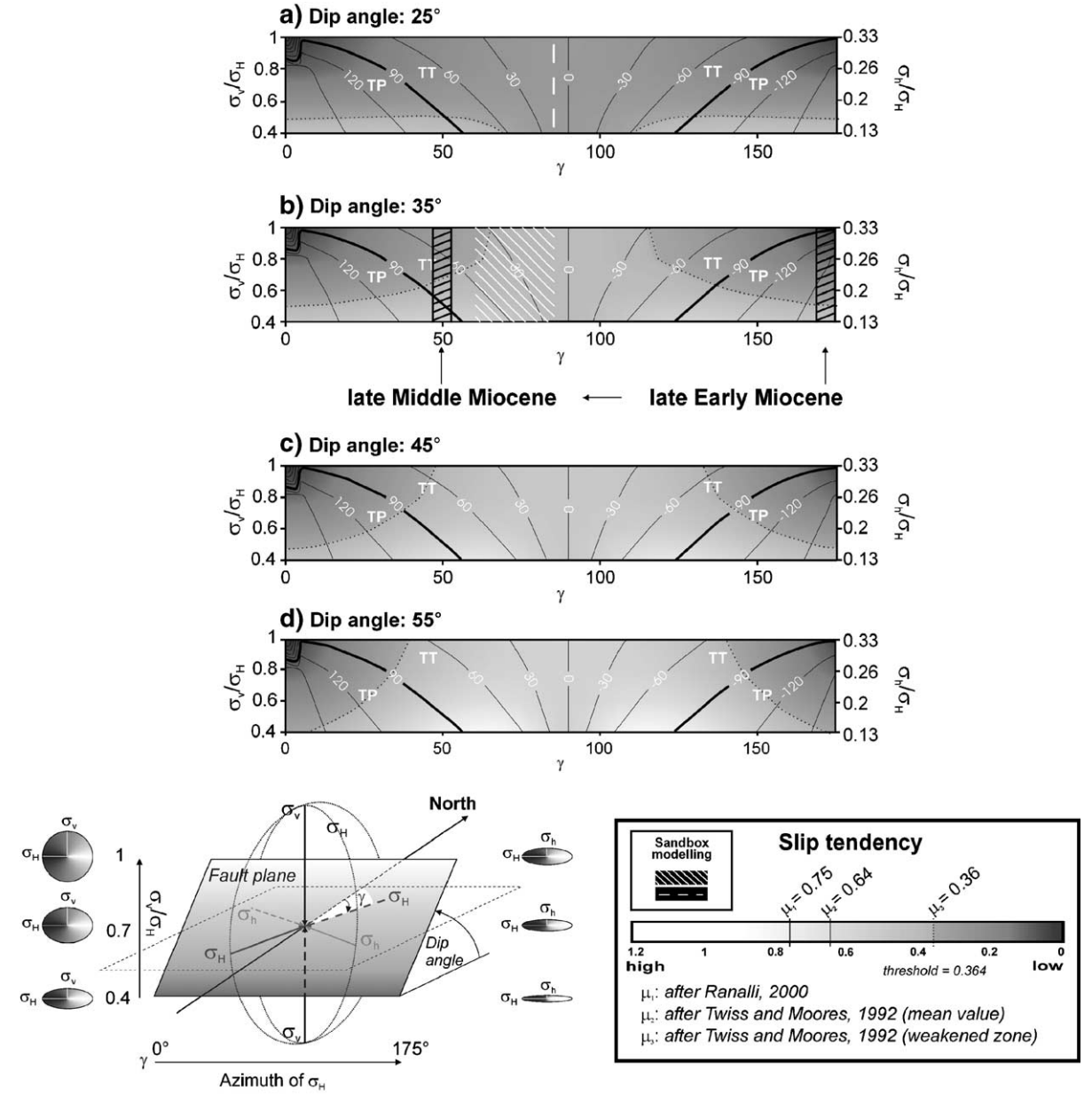

Fig. 11. Results of numerical modelling of fault reactivation in a strike-slip type stress field ($\sigma_H > \sigma_v > \sigma_h$). The ratio of σ_h/σ_v is kept constant (Case 1). For convenience, the fault is dipping to the south. The azimuth of the maximum horizontal stress direction ($0^\circ \le \gamma \le 175^\circ$) is on the horizontal axis, while the ratios of σ_v/σ_H and σ_h/σ_H are on the vertical axis. Reactivation pattern is analysed through seven steps as a function of the dip angle of the fault. Greyscale colouring shows slip tendency values, dashed line indicate the selected threshold value of 0.364. Other frictional angle values taken from the literature are also shown in the legend. Contour lines indicate slip direction on the fault plane, where 0°, 90° and -90° refer to normal, left lateral and right lateral faulting, respectively. Between these extremes, values of 0° to 90° and -90° to 0° indicate sinistral or dextral transtension (TT), respectively. Values above 90° and below -90° refer to transpression (TP) with sinistral and dextral component, respectively. Dashed white lines and white hatched areas show parameters of the sandbox experiments. Note that the figure is not symmetrical, since the horizontal scale is from 0° to 175°. Sketch in the lower left corner shows the spatial distribution of the fault plane and the stress ellipsoid. The small grey ellipsoids on both sides of the sketch represent stress ratios.

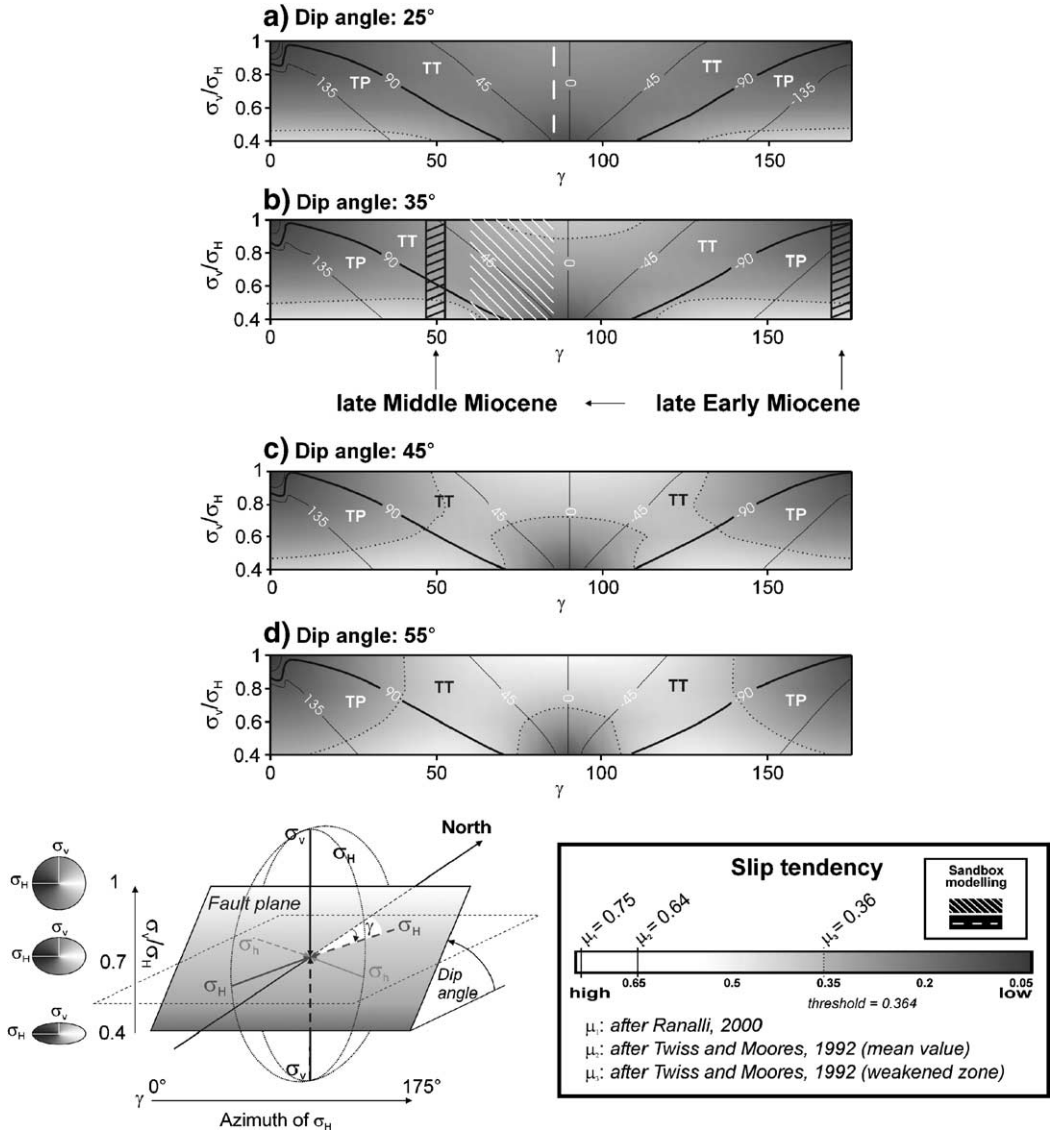

Fig. 12. Results of numerical modelling of fault reactivation in a strike-slip type stress field ($\sigma_H > \sigma_v > \sigma_h$). The ratio of σ_h/σ_H is kept constant (Case 2). For convenience, the fault is dipping to the south. The azimuth of the maximum horizontal stress direction ($0^\circ \leq \gamma \leq 175^\circ$) is on the horizontal axis, while the ratio of σ_v/σ_H is on the vertical axis. Reactivation pattern is analysed through seven steps as a function of the dip angle of the fault. Greyscale colouring shows slip tendency values, dashed line indicate the selected threshold value of 0.364. Other frictional angle values taken from the literature are also shown in the legend. Contour lines indicate slip direction on the fault plane, where 0°, 90° and -90° refer to normal, left lateral and right lateral faulting, respectively. Between these extremes, values of 0° to 90° and -90° to 0° indicate sinistral or dextral transtension (TT), respectively. Values above 90° and below -90° refer to transpression (TP) with sinistral and dextral component, respectively. Dashed white lines and white hatched areas show parameters of the sandbox experiments. Note that the figure is not symmetrical, since the horizontal scale is from 0° to 175°. Sketch in the lower left corner shows the spatial distribution of the fault plane and the stress ellipsoid. The small grey ellipsoids on the left side of the sketch represent stress ratios.

reactivation. The program uses the above mentioned hypothesis of Wallace (1951) and Bott (1959). As input the 3D fault geometry and, furthermore, 3 stress parameters are requested. These are the ratios of the minimum horizontal (σ_h) and the vertical (σ_v) stress with respect to σ_H (maximum horizontal stress) and, moreover, the azimuth value of the maximum horizontal stress direction (γ with respect to either the north or the strike of the fault under examination. Wórum et al. (2004) demonstrated that these values well represent the 3D stress field below a certain depth. In our study, a wide variety of synthetic faults has been analysed in order to investigate fault reactivation. For convenience, the dip of the fault planes is

to the south, while their dip angle is changing from 0° to 60° with 5° increments.

As output, we can obtain the slip tendency value that is related to the possibility of slipping, and the slip direction (SD) that is the direction of the motion with respect to the local dip of the fault plane. SD is supposed to occur in the direction of the maximum shear stress on the fault plane (Wallace's and Bott's hypothesis). Calculated slip directions vary from −180° to 180. 0° and 180° refer to normal (dip slip) and reverse faulting, respectively. 90° and −90° refer to left and right lateral fault kinematics, respectively. Slip direction values <90° and ≥90° refer to transtension, whereas values of 90° to 180° and −90° to −180° refer to transpression. In Figs. 10, 11 and 12, the greyscale colouring shows slip tendency values, while the contour lines indicate slip direction values. For further details of the modelling procedure and the mathematical background of the code, see Wórum et al. (2004).

In essence, the purpose of the numerical analysis was to calculate how the slip tendency and slip direction values vary as a function of the applied stress field, i.e. the magnitude of the differential stress, and the 3D orientation of the fault with respect to the confining stress field.

4.2. Modelling results

4.2.1. Thrust fault reactivation in extension

The relation of the stress magnitudes in extensional stress regime is: $\sigma_v > \sigma_H > \sigma_h$. In the simulation, the applied stress field was modified in six increments by changing the σ_h/σ_H ratio from 0.38 up to 0.95 and changing the σ_v/σ_H ratio from 1.14 up to 2.85. At the same time, the ratio of the least and largest stress (σ_h/σ_v) was kept at a constant value of 1/3. These values may reflect the paleostress values at the beginning and during the early development of the Danube basin (Fodor et al., 1999). When this area was highly elevated (i.e. bearing high gravitational potential energy), the vertical stress integrated over the thickness of the lithosphere could have exceeded the regional horizontal compression by a factor of 2 to 3. The selected σ_v/σ_H and σ_h/σ_v stress ratios represent a wide range of extensional stress fields observed in the Earth's crust. Modelling results are presented in Fig. 10 where only cases with 35° to 60° dip angle values are shown.

4.2.1.1. Slip tendency. ST values show great variability as a function of both the state of stress and the 3D orientation of the pre-defined fault plane (Fig. 10, colouring). The comparison of the four images in Fig. 10 reveals that ST values increase with increasing dip angle. It follows from simple mechanical considerations as well as from the results of analogue modelling that maximum likelihood of reactivation can be expected when the dip angle of the fault is ca. 60° (Fig. 10d). In this case, the maximum of ST values is 0.557. It is interesting to note that in cases with dip angle of 35° through 60°, the maximum ST values always coincidence with $\gamma = 90°$, independently from the applied stress ratio. In other words, ST values increase when the state of stress is fixed and γ is increasing. Fixing the γ value and increasing the stress ratios, the slip tendency gets also higher, at least at faults with up to ca. 60° dip angle (Fig. 10a to d). In case of sufficiently high stress ratio, the probability of reactivation is high. In summary, the more optimal the dip angle is (ca. 60°), the greater range of reactivation can be expected.

4.2.1.2. Slip direction. Calculated SD values show a gradual change with the dip angle of the pre-defined fault (Fig. 10, contour lines). Values typically range from −60° to 60° (transtension, i.e. normal faulting with strike-slip component), up to 60° of fault dip. In other words, the likelihood of strike-slip movement increases by increasing the dip of the pre-existing fault and by decreasing the stress ratios. On the other hand, selecting one dip angle from the model series, one can see that the maximum of SD values is at 35–45° of γ, practically at every state of stress.

4.2.2. Thrust fault reactivation in strike-slip stress regime

The relation of the stress magnitudes in strike-slip stress regime is: $\sigma_H > \sigma_v > \sigma_h$. A series of runs were made to carry out detailed parameter analysis. In case 1, we changed the σ_h/σ_H ratio from 0.133 up to 0.33, and the σ_v/σ_H ratio from 0.4 up to 1. Then in case 2, the σ_h/σ_H ratio remained constant (1/3), while the σ_v/σ_H ratio was changed from 0.4 up to 1 (similar to case 1). The stress ratios used in these modelling series are believed to reflect the paleostress conditions at time of the formation and mid-Miocene evolution of the Derecske trough (Fodor et al., 1999). In addition, the selected stress ratios represent a wide enough range of strike-slip type stress fields observed in the Earth's crust. Both case 1 and case 2 focus on how the ST and SD values change mainly as a function of the relative magnitude of σ_H and σ_v, respectively. Through these two cases, we aimed at investigating fault reactivation mechanics in the strike-slip stress domain. This series of models is meant to complement the previous set with extension in order to provide a full spectrum of

slip analysis and reactivation potential of pre-existing fractures. Modelling results are presented in Figs. 11 and 12 where cases with 25° up to 55° dip angle values are shown. A summary of the analysis is shown in Tables 6 and 7. In these tables, reactivation refers to the areas where slip tendency exceeds the selected threshold value of 0.364 (Twiss and Moores, 1992).

4.2.3. Case 1

4.2.3.1. Slip tendency. As a general trend, one can see in Fig. 11 that ST increases with the increasing dip of the pre-existing fault. This pattern is different from that of the previous model series (extension) where the dip-dependence of ST was far more complex (Fig. 10). At low dip angles (Fig. 11a to c), the maximum of slip tendency is at low stress ratios and at a wide γ range (from 0° to 60° and from 130° to 175°). The comparison of ST values in Figs. 10 and 11 suggests that in strike-slip stress regimes slipping or reactivation occur far more likely than under extension. The minimum values of ST are at high stress ratios and at $\gamma=0°$ and $\gamma=175°$, i.e. when σ_H is (almost) parallel to the strike of the fault. Fixing the γ value and increasing the stress ratio at a given dip angle, the ST values decrease. On the other hand, fixing the stress ratio and increasing γ up to 90°, the ST values increase.

4.2.3.2. Slip direction. The contour lines of slip direction show a complex pattern (Fig. 11, contour lines). Fixing the γ value at 40° and the dip value at 35° (Fig. 11b) and increasing the stress ratio, the slip direction gradually changes from transpression (SD>90°) to transtension (SD<90°) passing the SD value of 90°, which is the pure strike-slip movement, at the σ_v/σ_H ratio of ca. 0.8. Fixing the stress ratios in the same model and changing the γ value from 0° to 90°, SD changes from pure thrusting (SD=180°) through pure strike-slip (SD=90°) to normal faulting (SD=0°). Interestingly enough, the upper left corners of the figures show odd pattern regarding the slip direction. The maximum horizontal stress and the vertical stress magnitudes are nearly equal at that part of the parameter space. Moreover, the maximum horizontal stress is in the plane of the dip of the fault, therefore the minimum horizontal stress is in the plane of the fault. This situation means an unstable stress field ($R=1$) according to Larroque et al. (1987), suggesting either normal faulting or strike-slip faulting or any combination of these two cases.

Table 7
Summary of thrust fault reactivation analysis in strike-slip manner as a function of the dip angle, stress ratio and γ (the angle between the north and σ_H) of the pre-existing fault, using numerical modelling

γ value is around 90°	σ_v/σ_H high	Reactivation: normal faulting
	σ_v/σ_H low	No reactivation
γ value is around 0°	σ_v/σ_H high	No reactivation
	σ_v/σ_H low	Reactivation: transpression

In the table reactivation refers to the areas where slip tendency exceeds the threshold value of 0.364. The σ_h/σ_H ratio remained constant (1/3), while the σ_v/σ_H ratio was changed from 0.4 up to 1.

4.2.4. Case 2

The principle aim of this model series was to examine how the changing σ_v/σ_H ratio and σ_v itself influence the ST and SD values in a strike-slip stress regime. As the σ_h/σ_H ratio is fixed at 1/3, σ_h/σ_v values vary; all other modelling parameters are the same (Fig. 12).

4.2.4.1. Slip tendency. Increasing the dip of the pre-existing fault, the area of high ST values rapidly increases, as it was seen in the previous run (case 1). From 25° to 55° of dip angle (Fig. 12a to d), fixing a high stress ratio the ST increases with increasing γ values. Fixing a certain low γ value and increasing the stress ratio, the ST values decrease. However, when fixing a high γ value in the same model, ST increases. On the other hand, increasing the dip angle, slip tendency becomes more and more independent from the stress ratio at every γ value.

4.2.4.2. Slip direction. In contrast with case 1, SD values are quite insensitive to the change of the dip angle of the pre-existing fault (Fig. 12, contour lines).

Table 6
Summary of thrust fault reactivation analysis in strike-slip manner as a function of the dip angle, stress ratio and γ (the angle between the north and σ_H) of the pre-existing fault, using numerical modelling

γ value is around 90°	σ_v/σ_H and σ_h/σ_H high	Reactivation: normal faulting
	σ_v/σ_H and σ_h/σ_H low	Reactivation: transtension
γ value is around 0°	σ_v/σ_H and σ_h/σ_H high	No reactivation
	σ_v/σ_H and σ_h/σ_H low	Reactivation: transpression

In the table, reactivation refers to the areas where slip tendency exceeds the threshold value of 0.364.
The σ_h/σ_v ratio was kept at a constant value of 1/3, while the σ_h/σ_H ratio changed from 0.133 up to 0.33 and the σ_v/σ_H ratio from 0.4 up to 1.

Areas of transpression are characterised by low γ values at all stress ratios and higher γ values (up to 60°) with low stress ratios. Areas of transtension are at high γ values at all stress ratios and at lower γ values (down to 20°) with high stress ratio. These areas are evenly distributed in all of the models. The SD=−45° and SD=45° contour lines are getting at higher angles by increasing the dip angle. The domains of transtension and transpression are permanent in all the models, i.e. the 90° SD contour line has a fixed position at every dip angle. In these figures, the upper left corners of the figures also show odd pattern regarding the slip direction. The explanation is the same as in case 1.

5. Discussion

A series of analogue and numerical modelling experiments have been performed in order to examine how the compressional structures in the basement of the Pannonian basin influenced basin formation and subsequent tectonic evolution. The Pannonian lithosphere is made up of two main tectonic terrains, the ALCAPA and Tisza-Dacia terranes in the north and south, respectively (Fig. 1). The basement of these units consists of nappe piles formed during Cretaceous shortening in the Alpine orogen. The related compressional structures, affecting the style and basin geometry, played a key role in the subsequent phases of Miocene extension that eventually led to the formation of the back-arc type Pannonian basin. The style of deformation within the basin system shows great variability. Two end members, i.e. the Danube basin of pure extensional origin in the west and the Derecske trough of pull-apart origin in the east, were selected for the calibration and interpretation of our modelling study. The modelling has been also meant to improve and support the understanding of the origin of the two above-mentioned basins. Below, we present a discussion of the obtained results focusing on what we have learnt about thrust fault reactivation under subsequent extension. In addition, we present new insights on the mechanics of basin formation and deformation in the Pannonian basin.

5.1. Comparison of analogue and numerical models

It cannot be overemphasised that the analogue experiments took place at very low stress values. For this reason, the internal friction angle is highly variable and can considerably influence the modelling results. The internal friction angle is the main control on the angle between a failure plane (fault) and the maximum principle stress. Therefore, the results of the sandbox experiments have to be interpreted with care. In the case of numerical modelling, the threshold values of slip tendency also need caution. Due to its critical dependence on the frictional parameters, the calculated ST values cannot be directly related to actual fault reactivation. Instead, it is more reasonable if the ST pattern is compared with a reasonable range of frictional coefficients. With this approach, the accuracy of the reactivation pattern decreases, but its reliability increases. The presented values are considered to be valid along most faults and, thus, give a good insight into the reactivation potential as a function of the mechanical parameters of the fault plane. In other words, if the obtained ST overcomes an assumed frictional coefficient of the given fault before the mean stress becomes so high that a new fault could develop, the probability of repeated slip or reactivation is predicted to be high. The lowest threshold value (0.364) was adopted after Twiss and Moores (1992). Higher values (e.g. Ranalli, 2000) are also indicated (see legends of Figs. 10, 11 and 12).

5.1.1. Thrust fault reactivation as normal fault

The attempt on thrust fault reactivation modelling has been successful both with analogue and numerical techniques. Using analogue modelling (in case of normal stress regime), we found that reactivation is possible from 35° up to 60° dip of the pre-existing fault. At values of 35° and 40°, the frictional resistance of the fault planes was too high for simple reactivation. Therefore, silicone putty was applied to the fault plane to make it weaker. This procedure can be presented in a Mohr-diagram (Fig. 13). The frictional resistance of the intact sand is the highest (uppermost failure envelope marked by dashed line). The pre-existing fault has lower frictional resistance (intermediate failure envelope), whereas the FR of the pre-existing fault was lowered considerably by putting silicone putty on it (lowermost failure envelope). The Mohr-circle with continuous line marks the start of the experiment with the dip angles of two pre-existing faults, one without and one with silicon putty at $\theta_1=45°$ and $\theta_2=35°$, respectively (continuous lines). Both of them are able to reactivate on the failure envelope of the pre-existing fault without and with silicone putty on them, respectively (stage 1). When decreasing the dip angle from $\theta_1=45°$ to $\theta_1'=40°$ (dashed fault angle line in Fig. 13) and increasing the diameter of the Mohr-circle, it can reach the failure envelope of an intact rock, i.e. a new fracture forms (stage 2). In other words, a new fault forms instead of

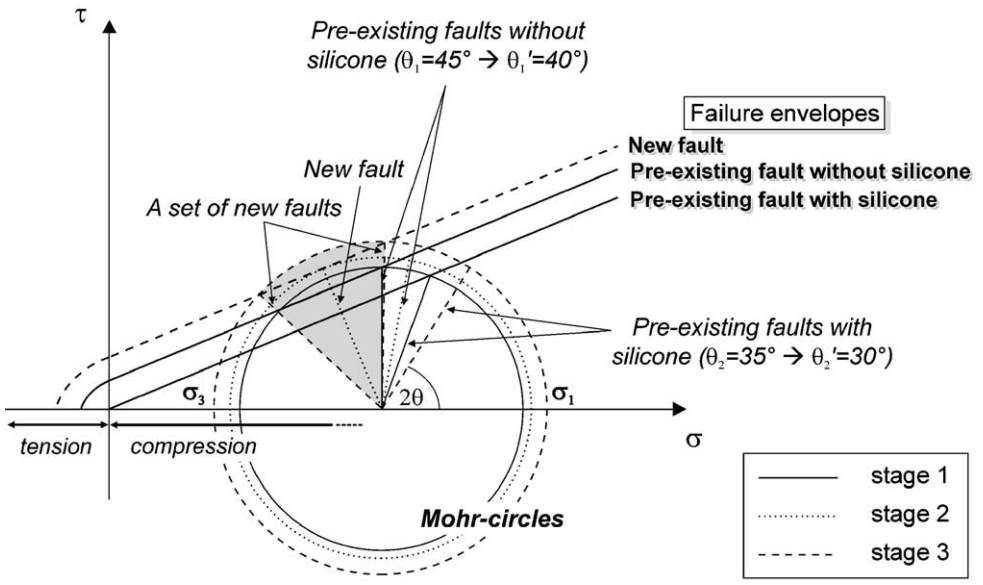

Fig. 13. Mohr-diagram showing failure envelopes for new and pre-existing fractures with and without silicone putty. In the case of a (weakened) pre-existing fault the cutting of the failure envelope and the *y*-axis is closer to the origin; therefore a properly oriented fault can be reactivated instead of creation of a new fault.

reactivating the pre-existing one with 40° of dip angle. Similar is the case with the weakened pre-existing fault with silicone putty on it. In case of $\theta_2=35^\circ$ dip angle, the Mohr-circle can reach the weakened failure envelope, but in case of $\theta_2'=30^\circ$ the Mohr-circle also reaches the failure envelope of the intact rock. This way, a set of new faults may be created again instead of the reactivation of the pre-existing one (stage 3, Fig. 13).

Numerical modelling gives us a wider range of possibilities to simulate reactivation processes than it is possible with analogue models. One image in Figs. 10, 11 or 12 reflects roughly 180 different stress ellipsoids and fault orientations, which means a total of 2100 different cases considering all the models. In case of extension ($\sigma_1=\sigma_v$) and for fault dip angles up to ca. 60°, the highest probability of slipping and, thus, reactivation is at the area of $\gamma=90^\circ$ (σ_h is perpendicular to the fault) and at any stress ratios. At $\gamma=90^\circ$, the value of ST hardly changes by changing the stress ratios, that is to say practically independent from them. By placing the slip tendency threshold at 0.364, reactivation can be achieved from 35° to 60° dip angle. However, a good accordance with the results of analogue modelling can be achieved when the threshold value is increased up to 0.44. At this value, reactivation is unlikely on fault planes with 35° and 40° dip angle, as experienced in the sandbox models. In Fig. 10, the position of the analogue models in the numerical domain is indicated by black dashed lines.

5.1.2. Thrust fault reactivation in transtension

The main difference between the two sets of analogue models (extension vs. transtension) is that in case of transtension reactivation was achieved by pushing the sand block. This way, the sand layer representing the hanging wall block was kept under compression during the experiments and, hence, it was stronger. All the experiments with the chosen parameters have been successful, except one. At 10° dip angle and 5° of strike (γ), new faults formed instead of reactivation (experiment #22). These faults rooted in the silicone putty–wooden plate contact zone. The frequent occurrence of reactivation in the sandbox models suggests that, with these parameters, reactivation in a strike-slip stress regime is far more likely than in pure extension. This means that reactivation may occur at a much wider range of the dip and the strike of the pre-existing faults. It also predicts a more frequent occurrence of strike-slip faulting in extensional basins formed by the tectonic reactivation of a former compressional domain. As one can see in Fig. 1, this is very often the case in the Pannonian basin.

The parameter domain of the analogue models is shown on the figures of the numerical simulation by white dashed lines in Figs. 11a and 12a or by white hatched area in Figs. 11b and 12b. It is interesting to note that if we set the slip tendency threshold at 0.364, apparently only one of the numerical model runs (case 1, 35° dip angle) confirms the results of the analogue models. In case 2, when σ_h/σ_H was kept fixed at 1/3, hardly any reactivation occurred. Similarly, in case 1

(below 35° dip angle) there was also no reactivation at the chosen threshold value. In contrast, in case of analogue modelling reactivation took place (experiments #19, #20 and #21). This suggests, the stress ratio of σ_v/σ_H has to be low enough (0.33 or lower) to achieve reactivation in a strike-slip stress regime. Hydraulic fracturing from the Great Hungarian Plain shows that this above-mentioned ratio is realistic in strike-slip regimes (Gerner et al., 1999). The lower the dip angle, the lower this ratio must be for the reactivation of pre-existing faults in transtension. Similarly, in the analogue models σ_H had to be also increased substantially to reactivate the pre-existing fault.

5.2. Applications to the Pannonian basin

Both analogue and numerical modelling suggest complex fault mechanics and reactivation pattern of thrust faults. Among these, the dip angle of former thrusts seems to play a crucial role. However, the geometry of the thrust systems in the Danube basin and the Derecske trough are quite similar, although the scale is somewhat different (compare Figs. 3 and 4). It is especially true for the upper segment of the Mihályi High (Danube basin) and the Palaeozoic fragment (Derecske trough) reached by an exploration well in the middle of the profile. Here, both the flat and the steeper parts (ramps) of a flat-ramp-flat thrust system can be observed. Considering this geometry, we propose a deformation scheme where the flat segments have not been reactivated. Instead, they are cut by normal faults rooting in the reactivated ramp segments of the thrust system (Fig. 14). This reactivation scheme does not explain, however, the strikingly different style of deformation in the two depressions of the Pannonian basin. In spite of the similar basement geometry, the Danube basin of pure extensional origin is characterised by dip-slip normal faulting (Fig. 14, Drawing 2), whereas the Derecske trough is a typical pull-apart basin with substantial lateral displacements along its master faults (Horváth and Rumpler, 1984; Windhoffer et al., 2003a; Fig. 14, Drawing 3). By implementing our modelling results, in the following section we seek for plausible mechanical and geodynamic explanation for the discrepancies in the tectonic style and fault kinematics observed in the two selected study areas.

5.2.1. Danube basin

According to Tari (1996), the Danube basin is of dominantly extensional origin where low-angle normal faulting, in combination with the formation of a metamorphic core complex in the footwall, played a crucial role. The author listed 3 different types of interaction between the newly formed normal faults and the pre-existing thrusts, and proposed that at depth the new and steep normal faults merge with pre-existing low-angle compressional structures. We can also assume that during the development of a metamorphic core complex the thrusts become steeper due to the uplift of the core as footwall. This makes thrust reactivation more likely. During subsequent basin development, block rotation of hanging wall units may have caused flattening and, thus, blocking extensional reactivation of these extensional structures.

Besides the geometry of the various segments of the thrust system, the state of stress must have played a crucial role as well. At the beginning of rifting in the Early Miocene, the area of the Danube basin was

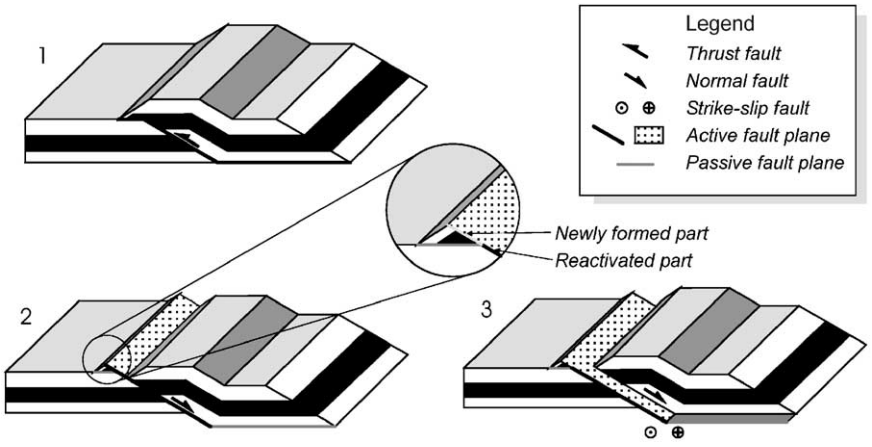

Fig. 14. Cartoon showing the proposed thrust fault reactivation styles. As it is suggested by analogue and numerical modelling the ramp part of the thrust system can be reactivated, while instead of reactivation of the flat parts new normal faults may cut the upper segments of the thrust system. (1) Simplified drawing of the original thrust system; (2) reactivation in pure extension; (3) reactivation in transtension.

characterised by an extensional stress regime with NNW–SSE directed compression ($\sigma_H=\sigma_2$) (Bada, 1999; Fodor et al., 1999). The angle between the strike of the compressional structures and the maximum horizontal stress direction was approximately 50° (i.e. $\gamma=40°$). On the other hand, the Danube basin was situated on top of the gravitationally collapsing and extruding Alpine orogen (sensu Bird, 1991; Ratschbacher et al., 1991; Tari, 1994; Bada and Horváth, 2001). This means a position of an area with high gravitational potential energy characteristic for most orogens. An important consequence is that the vertical stress magnitude ($\sigma_v=\sigma_1$) was most probably multiple of the two horizontal ones ($\sigma_H=\sigma_2$, $\sigma_h=\sigma_3$). Although net tension ($\sigma_v>\sigma_H$) is infrequently observed in the lithosphere, it is very characteristic for elevated orogens, as reported from, e.g. the Andes (Richardson and Coblentz, 1994), the Tibet plateau (Molnar and Tapponnier, 1978) and the western United States (Jones et al., 1996). Tension in these areas is the result of vertical buoyancy forces due to high topography exceeding the regional compressional stresses. These horizontal stresses are effectively decreased when the orogen has little or no lateral confinement (little or no Poisson effect). This was the case during the Miocene development of the Pannonian basin where the eastward retreat of the Carpathian subduction front provided open space in the Intra-Carpathian region available for extrusion of crustal-scale units from the axis of the east Alpine orogen (see Ratschbacher et al., 1991; Fodor et al., 1999). Therefore, the σ_v/σ_H ratio can be increased either by the higher vertical stresses integrated over the thickness of the lithosphere, or by the decrease of the prevailing horizontal compression or, most probably, by the complex interplay of these genetically related processes. Either way, the value of σ_v/σ_H must have increased substantially in the east Alpine orogen that could initiate the collapse of the mountain range. This in turn led to subsequent lithospheric extension in the form of rifting and basin formation. The reconstructed paleostress fields can be easily indicated on the diagram of the corresponding numerical models (see hatched areas in Fig. 10a and b). It is well visible that high slip tendency values are only at high stress ratios, i.e. when the vertical stress is large enough to initiate fault reactivation. Predicted slip direction is less than +5°, which is in very good agreement with the observed dip-slip normal faulting along the steeper segments of the thrust system (ramps). The positive value of SD refers to a small left-lateral component of fault displacement, in good agreement with observations (e.g. Fodor et al., 1999).

The differential topography of the collapsing orogen had relaxed by the end of the Early Miocene, as evidenced by marine sedimentation in the entire Pannonian basin. On the other hand, the stress pattern changed significantly in the Middle Miocene. Rotation of the paleostress field took place in the Danube basin and the angle between σ_H and the strike of the thrust system was reduced to 20° that in the numerical models corresponds to $\gamma=70°$ (see hatched areas in Fig. 10a and b). ST values are even higher than in the previous phase, SD values are again around +5° (dip-slip with sinistral component). The sandbox models indicate that further slip may have been facilitated by a reduced friction on the fault plane (e.g. clay smear, overpressured fluid along the fault plane, etc.). Finally, at the end of the Middle Miocene the stress direction changed again (e.g. Fodor et al., 1999) and σ_H became nearly parallel to the strike of the thrusts ($\gamma=-10°$). This range of γ is almost ideal for repeated fault reactivation with less than −5° of slip direction, i.e. pure extension prevailed.

5.2.2. Derecske trough

As described above, the geometry of the Cretaceous thrusts in the Derecske trough is similar to that of the Danube basin. One can see gently dipping thrust sheets, most of them reactivated during the Middle Miocene, and a number of newly formed, steeper normal faults. It is possible that the thrust planes were steeper at the beginning of basin formation. As can be seen in the seismic profile (Fig. 4), there are three former (two of them are sub-horizontal) thrust that were not reactivated during the Miocene extensional events. We believe that these two sub-horizontal planes represent the flat segment of a flat-ramp-flat thrust system. As basin development progressed, block rotation led to the rotation of the faults within them so that the ramp parts were flattening, while the flat parts were tilting back.

Besides the geometrical similarities, there are important differences between the Derecske and Danube basins, mainly in their geodynamic position and, consequently, in the state of stress at the time of basin formation during the Miocene. The region of the Derecske trough was situated far from the elevated Alpine orogen and was characterised by a much smoother surface and Moho topography (Frisch et al., 1998). Accordingly, gravitational stresses played a moderate role in the rifting process and the ratio of σ_v/σ_H must have been much lower than in the case of the Danube basin. Moreover, due to the proximity of the retreating Carpathian subduction front, the minimum horizontal stress σ_h must have been also signifi-

cantly reduced. All this resulted in a strike-slip type stress field ($\sigma_v=\sigma_2$) with NW–SE directed compression. The angle between the main strike of the compressional structures in the basement and σ_H (σ_1) was ca. −80° during the late Early Miocene as obtained from kinematic indicators from the neighbouring areas (e.g. Fodor et al., 1999). This corresponds to $\gamma=170°$ in the numerical models (see hatched areas in Figs. 11b and 12b), i.e. right-lateral transpression with very low probability of slipping. This is in sharp contrast with the sinistral transtensional origin of the Derecske trough. This discrepancy can be well explained by a somewhat delayed onset of rifting. After a rapid and significant rotation (up to 60°, Fodor et al., 1999) of the paleostress field, however, the angle between the thrusts and σ_H changed to around 40° by early Middle Miocene times ($\gamma=50°$). Numerical models suggest (Figs. 11b and 12b) that the fault–stress interaction results in a much higher value of ST and, thus, reactivation likelihood. In this stress domain, the master faults of the Derecske trough were acting as left-lateral faults with normal component (transtension).

Finally, the most prominent tectonic feature of the Derecske profile is the negative flower structure cross-cutting the entire Neogene–Quaternary sequence. This shear zone is connected to a recent reactivation of the basement structures, also suggested by seismicity data (Windhoffer et al., 2003a). This second phase of reactivation is attributed to the contemporaneous strike-slip type stress regime. The stress field has been slightly rotated with respect to the preceding Miocene–Pliocene one corresponding to $\gamma=60°$ (Figs. 11b and 12b). The numerical models predict sinistral strike-slip faulting with a normal component, consistent with the structural pattern observed on the seismic profile.

6. Conclusions

Analogue and numerical modelling has been carried out to obtain insights into the mechanics and kinematics of the reactivation pattern of compressional structures in general and, more particularly, in the basement of the Pannonian basin. Through this, we aimed to arrive at a better understanding of the complex rifting processes in the Pannonian basin system.

Both the analogue and numerical models suggest that thrust fault reactivation under pure extension is possible if the fault dip angle is larger than 45° with normal friction (e.g. sand on sand) on the fault plane. By making the fault plane weaker, reactivation is possible down to 35° of dip angle. Reactivation, however, is much easier in a strike-slip type of stress field. It can occur in a broad range of dip angles (35° through 20°) and strike angles (30° through 5° with respect to the direction of σ_H), provided the maximum horizontal stress is approximately three times larger in magnitude than the vertical or the minimum horizontal stresses.

The Cretaceous thrusts in the basement of the Pannonian basin have theoretically too low dip angles for reactivation under pure extension. Under certain circumstances, however, reactivation can be preferable to the formation of new high-angle normal faults. The flat-ramp-flat geometry of the thrust system allows the steeper parts (ramps) to reactivate, whereas the flat parts remain inactive or are abandoned. Instead of reactivation of the flat parts, which is mechanically unfavourable, new normal faults formed, nucleating in the reactivated ramp parts of the thrust system (Fig. 14).

In spite of all the similarities in the thrust geometry, the reactivation pattern is considerably different in the basement of the Danube basin and the Derecske trough (normal faulting in the Danube basin area vs. strike-slip faulting in the Derecske basin). Two main reasons are proposed for the observed dissimilarity. On one hand, the strike of the thrusts with respect to the maximum horizontal stress direction (σ_H) differs in the two areas. Besides this, their geodynamic position in the Pannonian basin was significantly different. At the onset of rifting in the Early Miocene, the Danube basin was situated on the elevated regions of the collapsing Alpine orogen and, thus, was characterised by an excess of gravitational potential energy. This resulted in high vertical stresses triggering the reactivation of thrusts (i.e. Alpine nappe boundaries) parallel to the development of metamorphic core complexes. Later in the Middle Miocene, when the region subsided under sea level, the paleostress field rotated and σ_h became perpendicular to the main strike of the thrusts facilitating further dip-slip normal faulting. On the contrary, the Derecske trough was located much closer to the Carpathian subduction front with no pronounced elevation and, thus, with low σ_v and with moderate σ_h magnitude values. Besides this, the oblique orientation of σ_H with respect to the reactivating thrusts was suitable for strike-slip faulting during the early Middle Miocene formation and the late Middle Miocene development of the basin.

Acknowledgments

The sandbox models described in this paper have been carried out in the Tectonic Laboratory (TecLab) of the Vrije Universiteit (VU), Amsterdam, the Netherlands. We thank Dimitrios Sokoutis and Maarten

Papo for their help and support. The numerical code applied in the paper was jointly developed by the VU and TNO-NITG (The Netherlands Institute of Applied Geoscience) supervised by Henk Pagnier. The first author thanks the European Union for his Marie Curie Eurobasin fellowship at the VU. We thank the Netherlands Research Centre for Integrated Solid Earth Science (ISES) for financial support and the Hungarian Scientific Research Fund (OTKA) projects no. F043715 and T034928. We are indebted to the journal reviewers M. Gölke and P. Richards for their constructive criticism and suggestions.

References

Ádám, O., Haas, J., Nemesi, L.R., Tátrai, M., Ráner, G., Varga, G., 1984. Geophysical investigations along geological key sections. Annu. Rep. Eötvös L. Geophys. Inst. Hung. 1983, 37–44 (in Hungarian with English abstract).

Anderson, E.M., 1951. The Dynamics of Faulting. Oliver and Boyd Ltd., Edinburgh. 206 pp.

Bada G., 1999. Cenozoic stress field evolution in the Pannonian basin and surrounding orogens. Inferences from kinematic indicators and finite element stress modelling. PhD thesis, Vrije Universiteit, Amsterdam. 204 pp.

Bada, G., Horváth, F., 2001. On the structure and tectonic evolution of the Pannonian Basin and surrounding orogens. Acta Geologica Hungarica 44/2–3, 301–327.

Balla, Z., 1984. The Carpathian loop and the Pannonian basin. A kinematic analysis. Geophysical Transactions 30, 313–353.

Bergerat, F., 1989. From pull-apart to the rifting process: the formation of the Pannonian Basin. Tectonophysics 157, 271–280.

Bird, P., 1991. Lateral extrusion of lower crust from under high topography, in the isostatic limit. Geophysical Research Letters 96, 10275–10286.

Bott, M.H.P., 1959. The mechanics of oblique slip faulting. Geological Magazine 96, 109–117.

Cloetingh, S., Lankreijer, A., 2001. Lithospheric memory and stress field controls on polyphase deformation of the Pannonian basin–Carpathian system. Marine and Petroleum Geology 18, 3–11.

Csontos, L., 1995. Tertiary tectonic evolution of the Intra-Carpathian area: a review. Acta Vulcanologica 7, 1–13.

Csontos, L., Nagymarosy, A., 1998. The mid-Hungarian line: a zone of repeated tectonic inversions. Tectonophysics 297, 51–71.

Csontos, L., Vörös, A., 2004. Mesozoic plate tectonic reconstruction of the Carpathian region. Palaeogeography, Palaeoclimatology, Palaeoecology 210, 1–56.

Fodor, L., Csontos, L., Bada, G., Benkovics, L., Györfi, I., 1999. Tertiary tectonic evolution of the Carpatho-Pannonian region: a new synthesis of paleostress data. In: Durand, B., Jolivet, L., Horváth, F., Séranne, M. (Eds.), The Mediterranean Basins: Tertiary Extension within the Alpine Orogen, Geol. Soc. London Spec. Publ., vol. 156, pp. 295–334.

Frisch, W., Kuhleman, J., Dunkl, I., Brügel, A., 1998. Palinspastic reconstruction and topographic evolution of the Eastern Alps during the late Tertiary tectonic extrusion. Tectonophysics 297, 1–15.

Gerner, P., Bada, G., Dövényi, P., Müller, B., Oncescu, M.C., Cloetingh, S., Horváth, F., 1999. Recent tectonic stress and crustal deformation in and around the Pannonian Basin: data and models. In: Durand, B., Jolivet, L., Horváth, F., Séranne, M. (Eds.), The Mediterranean Basins: Tertiary Extension within the Alpine Orogen, Geol. Soc. London Spec. Publ., vol. 156, pp. 269–294.

Horváth, F., 1993. Towards a mechanical model for the formation of the Pannonian basin. Tectonophysics 225, 333–358.

Horváth, F., Royden, L., 1981. Mechanism for formation of the intra-Carpathian basins: a review. Earth Evolution Sciences 1, 307–316.

Horváth, F., Rumpler, J., 1984. The Pannonian basement: extension and subsidence of an alpine orogene. Acta Geologica Hungarica 27 (3–4), 229–235.

Horváth, F., Bada, G., Szafián, P., Tari, G., Ádám, A., Cloetingh, S., in press. Formation and deformation of the Pannonian basin: constrains from observational data. In: Gee, D.G., Stephenson, R. (Eds.), European Lithosphere Dynamics. Geol. Soc. London Memoirs.

Hubbert, M.K., 1937. Theory of scale models as applied to the study of geologic structures. Geological Society of America Bulletin 48, 1459–1520.

Ivins, E.R., Dixon, T.H., Golombek, M.P., 1990. Extensional reactivation of an abandoned thrust: a bound on shallowing in the brittle regime. Journal of Structural Geology 12/3, 303–314.

Jaeger, J.C., Cook, N.G.W., 1976. Fundamental of Rock Mechanics. Chapman & Hall, London. 513 pp.

Jones, C.H., Unruh, J.R., Sonder, L.J., 1996. The role of gravitational potential energy in active deformation in the southwestern United States. Nature 381, 37–41.

Kováč, M., Král, J., Márton, E., Plašienka, D., Uher, P., 1994. Alpine uplift history of the Central Western Carpathians: geochronological, paleomagnetic, sedimentary and structural data. Geologica Carpathica 45, 83–96.

Lankreijer, A., Bielik, M., Cloetingh, S., Majcin, D., 1999. Rheology predictions across the western Carpathians, Bohemian massif, and the Pannonian basin: implications for tectonic scenarios. Tectonics 18, 1139–1153.

Larroque, J.M., Etchecopar, A., Philip, H., 1987. Evidence for the permutation of stresses σ_1 and σ_2 in the Alpine foreland: the example of the Rhine graben. Tectonophysics 144 (4), 315–322.

McClay, K., Massimo, B., 2001. Analog models of restraining stepovers in strike-slip systems. AAPG Bulletin 85 (2), 233–260.

Molnar, P., Tapponnier, P., 1978. Active tectonics of Tibet. Journal of Geophysical Research 83, 5361–5374.

Morris, A., Ferrill, D.A., Henderson, D.B., 1996. Slip-tendency analysis and fault reactivation. Geology 24 (3), 275–278.

Ranalli, G., 2000. Rheology of the crust and its role in tectonic reactivation. Journal of Geodynamics 30, 3–15.

Ratschbacher, L., Merle, O., Davy, P., Cobbold, P., 1991. Lateral extrusion in the Eastern Alps: Part 1. Boundary conditions and experiments scaled for gravity. Tectonics 10, 245–256.

Richard, P.D., Naylor, M.A., Koopman, A., 1995. Experimental models of strike-slip tectonics. Petroleum Geoscience 1, 71–80.

Richardson, R.M., Coblentz, D.D., 1994. Stress modeling in the Andes: constraints on the South American intraplate stress magnitudes. Journal of Geophysical Research 99, 22015–22025.

Royden, L.H., Horváth, F., Rumpler, J., 1983. Evolution of the Pannonian basin system: 1. Tectonics. Tectonics 2, 63–90.

Sibson, R.H., 1974. Frictional constraints on thrust, wrench and normal faults. Nature 249, 542–544.

Sibson, R.H., 1985. A note on fault reactivation. Journal of Structural Geology 7, 751–754.

Sibson, R.H., 2000. Fluid involvement in normal faulting. Journal of Geodynamics 29, 469–499.

Tari G., 1994. Alpine Tectonics of the Pannonian Basin. PhD thesis. Rice University, Houston, Texas. 501 pp.

Tari, G., 1996. Neoalpine tectonics of the Danube Basin (NW Pannonian Basin, Hungary). In: Ziegler, P.A., Horváth, F. (Eds.), Peri-Tethys Memoir 2: Structure and Prospects of Alpine Basins and Forelands, Mèm. Mus. Natn. Hist. nat., vol. 170, pp. 439–454. + Enclosures 1–3.

Tari, G., Horváth, F., Rumpler, J., 1992. Styles of extension in the Pannonian Basin. Tectonophysics 208, 203–219.

Tari, G., Báldi, T., Báldi-Beke, M., 1993. Paleogene retroarc flexural basin beneath the Neogene Pannonian Basin: a geodynamic model. Tectonophysics 226, 433–455.

Tari, G., Dövényi, P., Dunkl, I., Horváth, F., Lenkey, L., Stefanescu, M., Szafián, P., Tóth, T., 1999. Lithospheric structure of the Pannonian basin derived from seismic, gravity and geothermal data. In: Durand, B., Jolivet, L., Horváth, F., Séranne, M. (Eds.), The Mediterranean Basins: Tertiary Extension within the Alpine Orogen, Geol. Soc. London Spec. Pub., vol. 156, pp. 215–250.

Tchalenko, J.S., 1970. Similarities between shear zones of different magnitudes. Geological Society of America Bulletin 81, 1625–1640.

Twiss, R.J., Moores, E.M., 1992. Structural Geology. W. H. Freeman and Company, New York. 532 pp.

van Mechelen, D., Koekoek, G., Nieuwland, D.A., 2003. Surface tension effects on the shear strength of unsaturated granular materials. Interdisciplinary research project. Tectonic Laboratory of the Faculty of Earth and Life Sciences, Department of Tectonics and Structural GeologyVrije Universiteit, Amsterdam. 1–22 pp.

Wallace, R.E., 1951. Geometry of shearing stress and relation to faulting. Journal of Geology 59, 118–130.

Windhoffer, G., Bada, G., Horváth, F., Cloetingh, S., Szafián, P., Timár, G., 2003a. Pull-apart basin evolution and fault reactivation: a case study of the Derecske trough, Pannonian basin. Geophysical Research Abstracts 5, 04140.

Windhoffer, G., Wórum, G., Bada, G., Cloetingh, S., Horváth, F., 2003b. 3D numerical modelling of slip tendency of recently active strike-slip fault system, Derecske trough, Pannonian basin. The fourth Stephan Mueller conference of the European Geophysical Society: geodynamic and tectonic evolution of the Carpathian arc and its foreland: environmental tectonics and continental topography. Retezat Mountains, South Carpathians, Romania.

Wórum, G., Van Wees, J.D., Bada, G., Van Balen, R.T., Cloetingh, S.A.P.L., Pagnier, H., 2004. Slip tendency analysis as a tool to constrain faultreactivation: a numerical approach applied to 3D fault models in the Roer Valley Rift System (southeast Netherlands). Journal of Geophysical Research 109, B02401. doi:10.1029/2003JB002586.